

**Best  
Available  
Copy**

AD-760 390

INVESTIGATION OF OPTICAL GAIN IN GAS  
DYNAMIC LASER MEDIA

S. Russell, et al

United Aircraft Research Laboratories

Prepared for:

Air Force Weapons Laboratory  
Advanced Research Projects Agency

April 1973

DISTRIBUTED BY:

**NTIS**

National Technical Information Service  
U. S. DEPARTMENT OF COMMERCE  
5285 Port Royal Road, Springfield Va. 22151

AD 760390



## INVESTIGATION OF OPTICAL GAIN IN GDL MEDIA

S. Russell

R. A. Meinzer

United Aircraft Research Laboratories

TECHNICAL REPORT NO. AFWL-TR-72-217

April 1973

Reproduced by  
NATIONAL TECHNICAL  
INFORMATION SERVICE  
U S Department of Commerce  
Springfield VA 22151



**AIR FORCE WEAPONS LABORATORY**

**Air Force Systems Command**

**Kirtland Air Force Base**

**New Mexico**

Approved for public release; distribution unlimited.

AFWL-TR-72-217

PROJECT NO.	
FIG.	DATE SUBMITTED
FIG.	DATE SUBMITTED
UNCLASSIFIED	
JUSTIFICATION	
BY	
DISTRIBUTION/AVAILABILITY CODES	
Dist.	Avail. Group Special
A	

AIR FORCE WEAPONS LABORATORY  
Air Force Systems Command  
Kirtland Air Force Base  
New Mexico 87117

When US Government drawings, specifications, or other data are used for any purpose other than a definitely related Government procurement operation, the Government thereby incurs no responsibility nor any obligation whatsoever, and the fact that the Government may have formulated, furnished, or in any way supplied the said drawings, specifications, or other data, is not to be regarded by implication or otherwise, as in any manner licensing the holder or any other person or corporation, or conveying any rights or permission to manufacture, use, or sell any patented invention that may in any way be related thereto.

DO NOT RETURN THIS COPY. RETAIN OR DESTROY.

UNCLASSIFIED

Security Classification

## DOCUMENT CONTROL DATA - R &amp; D

(Security classification of title, body of abstract and indexing annotation must be entered when the overall report is classified)

1. ORIGINATING ACTIVITY (Corporate author) United Aircraft Research Laboratories 400 Main Street East Hartford, Connecticut 06118		2a. REPORT SECURITY CLASSIFICATION UNCLASSIFIED
		2b. GROUP
3. REPORT TITLE  INVESTIGATION OF OPTICAL GAIN IN GDL MEDIA		
4. DESCRIPTIVE NOTES (Type of report and inclusive dates) 22 September 1971 through 31 July 1972		
5. AUTHOR(S) (First name, middle initial, last name)  S. Russell and R. A. Meinzer		
6. REPORT DATE April 1973	7a. TOTAL NO. OF PAGES <del>95</del> 90	7b. NO. OF REFS 12
8a. CONTRACT OR GRANT NO. F29601-71-C-0053	9a. ORIGINATOR'S REPORT NUMBER(S)  AFWL-TR-72-217	
b. PROJECT NO. 1256	9b. OTHER REPORT NO(S) (Any other numbers that may be assigned this report)  L911115-18	
c.		
d.		
10. DISTRIBUTION STATEMENT  Approved for public release; distribution unlimited.		
11. SUPPLEMENTARY NOTES		12. SPONSORING MILITARY ACTIVITY AFWL (LRL) Kirtland AFB, NM 87117
13. ABSTRACT (Distribution Limitation Statement A)  An experimental program was conducted using a small-scale, arc-augmented gas-dynamic laser with the objective of obtaining comprehensive data for evaluating theoretical predictions of optical gain for such devices over a wide range of potential operating conditions. Included among the program results were attainment of stagnation temperatures higher than those possible in ordinary combustion-driven gas-dynamic lasers, experimental evaluation of the homogeneity of the flow in this device and theoretical determination of the plenum gas composition from the experimentally measured stagnation temperature and pressure. A number of experimental difficulties were encountered during this program which limited the scope of the gain measurements obtained and thereby partially compromised the overall program objective. Included among these difficulties were restrictions in test time due to the effort expended to make the equipment operational over the extended range of conditions, operational difficulties resulting from arc-current transients which caused excessive arc electrode erosion during starting, problems evolving from the condensation of this electrode material in the nozzle throat and possible uncertainties in the nozzle throat area.  Details of illustrations in this document may be better studied on microfiche.		

DD FORM 1473  
1 NOV 65UNCLASSIFIED  
Security Classification

14

KEY WORDS

LINK A

LINK B

LINK C

ROLE

WT

ROLE

WT

ROLE

WT

Lasers  
Gas Dynamic Lasers

ia

AFWL-TR-72-217

INVESTIGATION OF OPTICAL  
GAIN IN GDL MEDIA

S. Russell  
R. A. Meinzer

United Aircraft Research Laboratories

TECHNICAL REPORT NO. AFWL-TR-72-217

Approved for public release; distribution unlimited.

*1-6*

FOREWORD

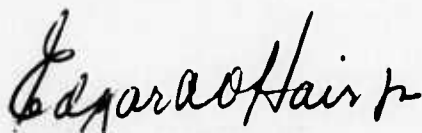
This report was prepared by the United Aircraft Research Laboratories, East Hartford, Connecticut, under Contract F29601-71-C-0053. The research was performed under Program Element 623011D, Project 1256, and was funded by the Advanced Research Projects Agency (ARPA) under ARPA Order 1256.

Inclusive dates of research were 22 September 1971 through 31 July 1972. The report was submitted 22 February 1973 by the Air Force Weapons Laboratory Project Officer, Captain Roger A. Miller (LRL).

This technical report has been reviewed and is approved.



ROGER A. MILLER  
Captain, USAF  
Project Officer



EDGAR A. O'HAIR, JR.  
Lt Colonel, USAF  
Chief, Laser Technology Branch



DONALD L. LAMBERSON  
Colonel, USAF  
Chief, Laser Division

## CONTENTS

<u>Section</u>	<u>Page</u>
I      SUMMARY	1
II     INTRODUCTION	3
III    FACILITY DESCRIPTION	6
1.   MINI-ROCKET TEST FACILITY	6
2.   ARC HEATER OPERATION	10
IV     EXPERIMENTAL WORK	14
1.   PHASE I	14
a.   Design of the Arc-Combustor- Nozzle Assembly	14
(1)   General Considerations	14
(2)   Arc-Combustor-Nozzle Design	17
(3)   Construction of Arc-Combustor- Nozzle Assembly	19
b.   Shake down tests of Assembly in Mini-Rocket Facility	20
(1)   Facility Problems	20
(2)   Temperature Homogeneity	23
(3)   Pressure Measurements	29
(4)   Gas Composition	31
(5)   Error Analysis	32
(6)   Equipment Reliability	36

## CONTENTS (Cont'd)

<u>Section</u>	<u>Page</u>
2. PHASE II	40
a. Gain Measurements	40
b. Analysis of Gain Measurements	46
V CONCLUSIONS AND RECOMMENDATIONS	51
APPENDICES	55
I. Details of Arc Operation	55
II. Conduction and Radiation Corrections to Thermocouple Readings	58
III. Nozzle Throat Area During Runs	60
IV. Equilibrium Calculations for Data Points in Test Matrix	63
V. Apparent Gain Reductions Resulting from the Doppler Effect	72
REFERENCES	76

# ILLUSTRATIONS

<u>Figure</u>		<u>Page</u>
1	Reaction Vessel	7
2	Control Panels for arc/power supply and gas flows	8
3	Gas Delivery System (Schematic)	9
4	Arc-Combustor-Nozzle Assembly (Diagram)	12
5	Arc Starter	13
6	Theoretical Stagnation Temperature attainable in GDL Mini-rocket without heat loss	16
7	Nozzle Assembly (Schematic)	21
8	Arc-Combustor-Nozzle Assembly (Photo)	22
9	High Temperature Thermocouple Installation	24
10	Run Temperature Profile during a Typical Run	26
11	Experimental Stagnation Temperatures	28
12	Run Pressure and Temperature Profiles	30
13	Variation of Error in Gain Measurements with the Magnitude of the Small Signal Gain	35
14	Anode Face After 15 runs	37
15	Cathode Face After 30 runs	38
16	Nozzle Throat After 10 runs	39
17	Configuration for Three Simultaneous Gain Measurements (Schematic)	42
18	Laser, Optical Bench, and Reaction Vessel Positioned for Gain Measurements	43
19	Gain Tracings, 10 cm location	44
20	Gain Tracings, 10 cm location	45

# ILLUSTRATIONS (Cont'd)

<u>Figure</u>		<u>Page</u>
21	Gain Versus Temperature for Arc Powered GDL	49
22	Gain-Pressure-Temperature Tracings	50
23	Voltage and Current traces during Arc Ignition	56
24	Nozzle Throat Area as a Function of Temperature	62
25	Variations in Combustor product composition corresponding to run conditions listed in Group 1 of Table I	64
26	Variations in Combustor product composition corresponding to run conditions listed in Group 2 of Table I	65
27	Variations in Combustor product composition corresponding to run conditions listed in Group 3 of Table I	66
28	Variations in Combustor product composition corresponding to run conditions listed in Group 4 of Table I	67
29	Variations in Combustor product composition corresponding to run conditions listed in Group 5 of Table I	68
30	Variations in Combustor product composition corresponding to run conditions listed in Group 6 of Table I	69
31	Variations in Combustor product composition corresponding to run conditions listed in Group 7 of Table I	70
32	Variations in Combustor product composition corresponding to run conditions listed in Group 8 of Table I	71
33	Normalized gain in the Doppler Region as a function of Frequency for $T = 300^{\circ}\text{K}$	74

## TABLES

<u>Table</u>		<u>Page</u>
I	Run Conditions	15
II	Temperature Homogeneity Across Nozzle	27
III	Experimental Gain Measurements	48

# SYMBOLS

$A$	Nozzle throat area
$C_D$	Nozzle discharge coefficient
$D$	Thermocouple wire diameter
$I$	Probe laser intensity after passage through GDL
$I_O$	Probe laser intensity
$I_s$	Saturation intensity
$L$	Optical path length
$M$	Free stream Mach number
$M_w$	Molecular weight
$P$	Static pressure
$P_O$	Stagnation pressure
$R$	Gas Constant
$T$	Temperature
$T_O$	Stagnation Temperature
$T_b$	Thermocouple support temperature
$T_d$	Equivalent duct temperature
$T_g$	Gas temperature
$T_w$	Indicated thermocouple temperature
$V$	Bulk gas velocity
$V_r$	Velocity of source
$W$	Weight flow
$X$	Mole fraction

# SYMBOLS (Cont'd)

$X_{CO}$	Mole Fraction of CO
$X_{CO_2}$	Mole Fraction of CO <sub>2</sub>
$X_{H_2O}$	Mole Fraction of H <sub>2</sub> O
$X_{N_2}$	Mole Fraction of N <sub>2</sub>
$Y$	Variable with cumulative error
$c$	Speed of light
$f$	Observed frequency
$f_0$	Frequency of stationary source
$g$	Gain
$g_0$	Small signal gain
$k_w$	Thermal conductivity of thermocouple wire
$\Sigma_g$	Effective emissivity of gas
$\Sigma_w$	Effective emissivity of thermocouple wire
$\alpha_{g, d}$	Effective absorptivity of gas for black-body radiation at temperature $T_d$
$\gamma$	Heat capacity ratio
$\theta$	Angle between probe laser and gas flow
$\lambda$	Wavelength
$\nu$	Frequency at which gain is measured
$\nu_0$	Center frequency of gain profile

## SECTION I

### SUMMARY

An experimental program was conducted using a small-scale, arc-augmented gas-dynamic laser (GDL) with the objective of obtaining comprehensive data for evaluating theoretical predictions of optical gain for such devices over a wide range of potential operating conditions. An existing combustion-driven GDL facility was augmented with a 530 kW arc-jet heater to provide stagnation temperatures unattainable by the combustion of ordinary liquid and gaseous reactants in an attempt to simulate conditions estimated for the combustion of solid propellants. The unmodified combustion-driven GDL facility had previously been employed for making extensive gain measurements and performance evaluations for conventional GDL configurations and had been well-characterized during these earlier test programs. Under the present program, stagnation temperatures higher than those reached in ordinary gas-dynamic lasers were obtained and measurements were made to indicate that an acceptable level of temperature homogeneity had been achieved to permit the theoretical determination of the plenum gas composition. This information was in turn used to assess the importance of the water-gas equilibrium which, for the conditions considered, dictates that excess carbon monoxide would result in significant concentrations of hydrogen and concomitant reduction in water concentration. In addition, limited gain measurements were made.

During the course of this program, a number of experimental difficulties were encountered which limited the scope of the gain measurements and, thereby,

partially compromised the overall program objective. Included among the difficulties were restrictions in test time due to the effort expended to make the equipment operational over the extended range of conditions, operational difficulties resulting from arc-current transients which caused excessive arc electrode erosion during starting, problems resulting from the condensation of electrode material in the nozzle throat and possible uncertainties in the nozzle throat area. The variances found in the gain traces were considerably larger than anticipated and much greater than had been recorded during pure combustion-driven GDL gain measurements. Part of this variability resulted from operational problems with the arc heater and instabilities in the probe laser. For example, the gain data obtained might be suspect because of the possibility that eroded copper metal might have contaminated the gases. However, since most of the erosion noted occurred during starting current transients, relatively little copper vapor was present during the part of test when the gain was measured. Furthermore, post run inspections gave qualitative evidence of the presence of copper in and upstream of the nozzle throat and also within the combustor; no evidence of copper deposits downstream of the nozzle throat was found. The difficulty with electrode lifetime was traced to shortcomings in the arc power supply and attempts to rectify the situation during the course of the program were not totally satisfactory.

## SECTION II

### INTRODUCTION

In conventional gas-dynamic laser (GDL) configurations, gaseous reactants are combusted in the appropriate proportions to generate an optimum active medium. It is clear that the performance of such lasers would be improved if higher stagnation temperature could be achieved. One possible means to obtain increased stagnation temperature is the use of solid propellant fuels. Such use would also be significant in the development of minimum weight, compact devices, which would have long shelf life.

To aid in the development of the appropriate solid propellants, information is required on the magnitude of the optical gain which can be achieved with various hypothetical formulations. Since the combustion of solid propellants tends to generate significant concentrations of carbon monoxide, as well as high stagnation temperatures, little data are available on the anticipated gain as indicated in references 1-9. The magnitude of the gain can be estimated using various theoretical models, but these models have received relatively little experimental validation at the conditions corresponding to those anticipated from the burning of solid propellants. Therefore, the objective of the program described herein was to perform a series of comprehensive gain measurements in a small-scale, arc-jet augmented GDL using gas compositions at temperatures representative of those that might be achieved by the burning of solid propellants so that the performance potential of such systems might be established and the predictions of various theoretical models validated.

25

The research program was divided into two phases. Phase I entailed the design and fabrication of an arc-combustor-nozzle assembly, its installation in United's "mini-rocket" GDL test facility, (reference 9), and a comprehensive evaluation of the suitability of the facility for making reliable gain measurements. This evaluation included the following:

- a. Determination of the temperature homogeneity upstream of the nozzle;
- b. Measurement of pressure fluctuations in the combustion chamber;
- c. Determination of the capability of the facility to achieve the desired run conditions (c.f. Phase II);
- d. Determination of the experimental procedures and equipment required to achieve the desired run conditions;
- e. Assessment of the reliability of the equipment, especially the arc heater;
- f. Performance of an error analysis to estimate the error associated with each critical run parameter, (i.e., stagnation temperature; stagnation pressure; mole fraction of  $\text{CO}_2$ ,  $\text{N}_2$ ,  $\text{H}_2\text{O}$  and  $\text{CO}$ ; distance downstream of the GDL nozzle; and optical gain).

Phase II of this program required the measurement or calculation of selected parameters at specific sets of run conditions. These parameters included:

- a. Optical gain, using a single frequency  $\text{CO}_2$  probe laser;
- b. Combustion chamber temperature, using high-temperature thermocouple probes;
- c. Combustion chamber pressure, using a pressure transducer;
- d. Gas composition, using a computer program available at UARL with

values of individual gas flow rates, stagnation temperature, and stagnation pressure as input data.

## SECTION III

### FACILITY DESCRIPTION

#### 1. MINI-ROCKET TEST FACILITY

The reaction vessel which houses the arc-combustor-nozzle assembly is a vacuum-tight stainless steel cylinder (twelve inches internal diameter) with gas and water feed-throughs in end and side flanges, (see figure 1). The arc-combustor-nozzle assembly, not visible in figure 1, is installed in the rear. The downstream end of the vessel is connected through appropriate piping and valves to a vacuum sphere having a volume of 4800 cubic feet. The vacuum-tight test facility protects laboratory personnel from exposure to carbon monoxide in the event of leaks in the test assembly, and the use of the large vacuum sphere permits runs, which were generally of the order of thirty seconds, to be made without increasing the pressure in the facility more than 10 to 12 torr.

Arc operation, cooling water flows, and gas flows were controlled from wall-mounted control panels located a short distance from the reaction vessel, (see figure 2). Appropriate safety devices against system over-pressurization, over-temperature, etc., were built into the control system.

A schematic of an individual gas delivery line is shown in figure 3. There are five such lines - two for nitrogen and one each for hydrogen, oxygen (or nitrous oxide), and carbon monoxide. The gas is supplied from high pressure cylinders joined by a manifold and located outside an exterior wall of the room. The outlet of the manifold has a single manual shut-off valve through which the

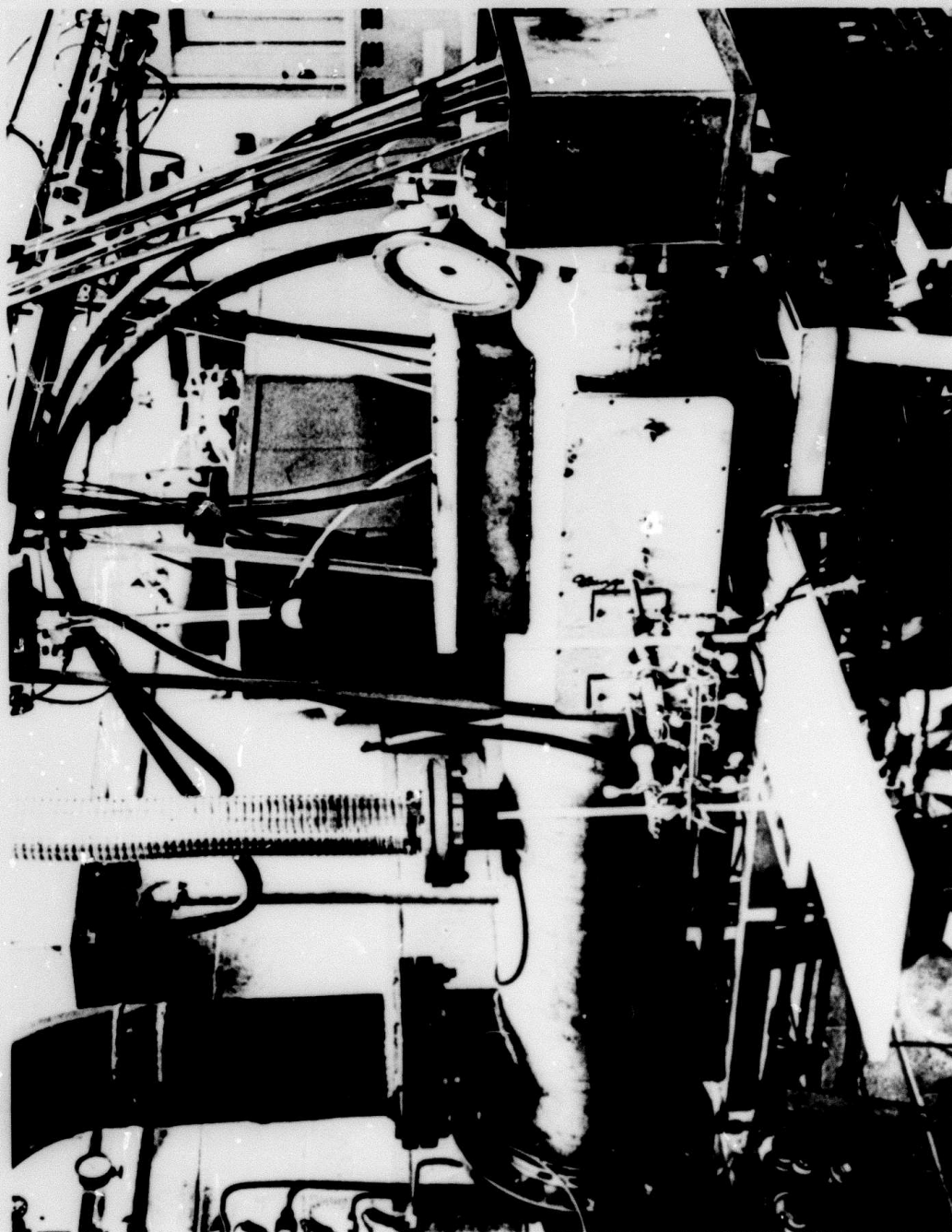


Figure 1. Reaction Vessel

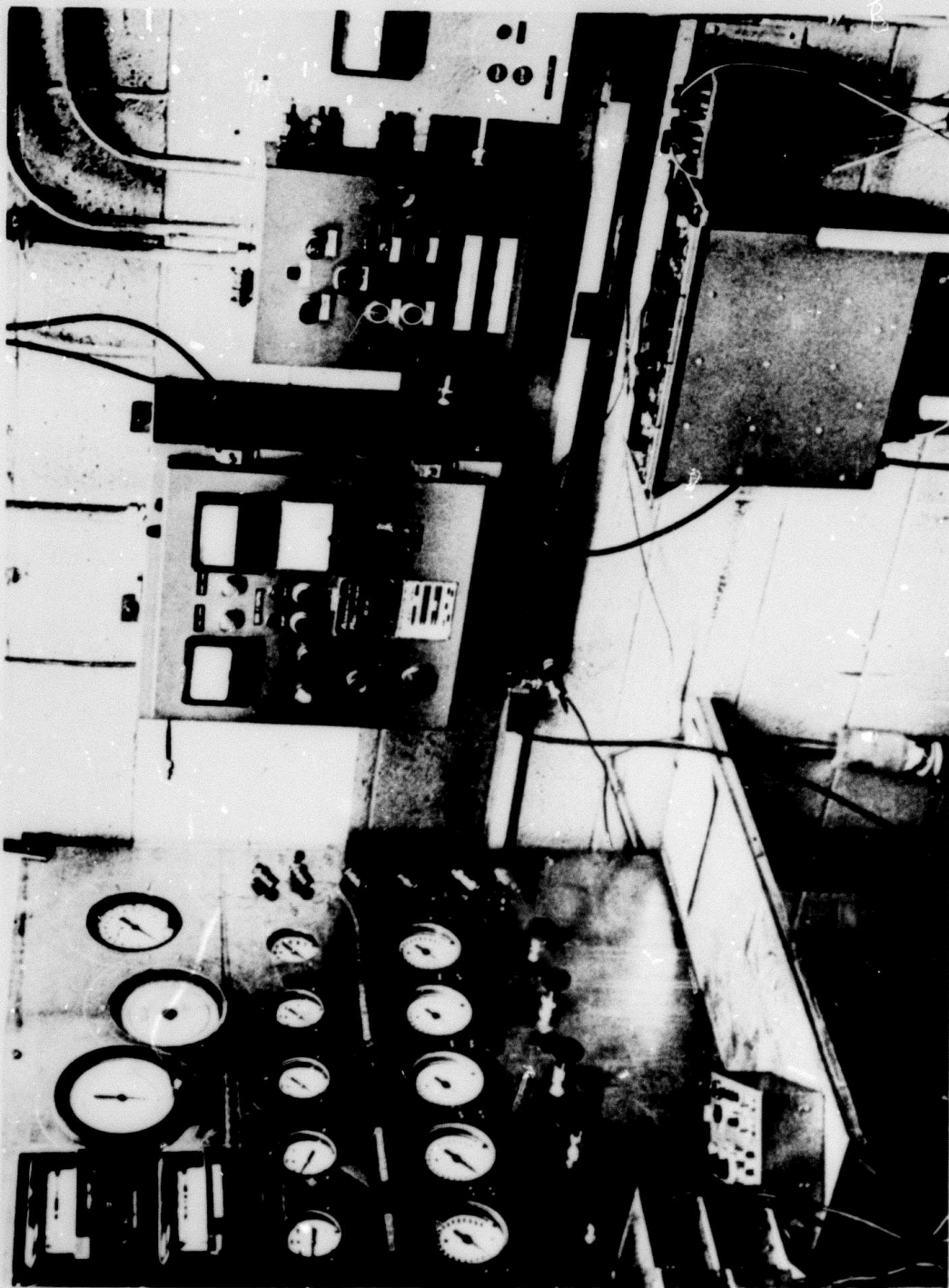
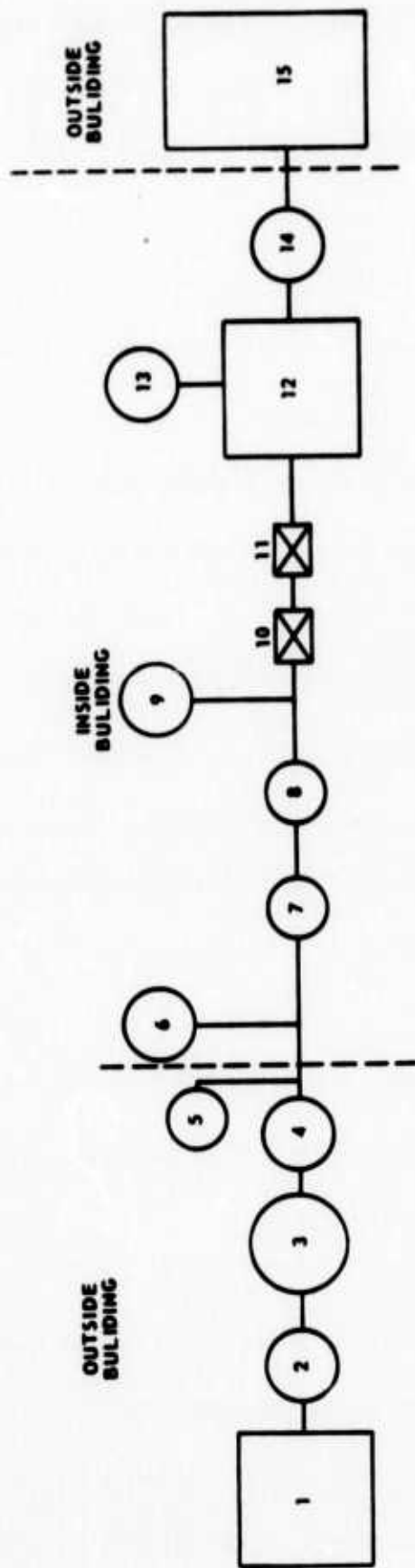


Figure 2. Control Panels for Arc/Power Supply and Gas Flows



- |                                |   |
|--------------------------------|---|
| 1 GAS CYLINDERS WITH MANIFOLD  | 9 PRESSURE GAUGE PRECEDING CHOKED ORIFICE |
| 2 MANUAL SHUT-OFF VALVE        | 10 CHOKED ORIFICE                         |
| 3 GAS PRESSURE REGULATOR       | 11 CHECK VALVE                            |
| 4 OUTSIDE SOLENOID VALVE       | 12 ARC-COMBUSTOR-NOZZLE ASSEMBLY          |
| 5 OUTSIDE MANUAL BLEED VALVE   | 13 PRESSURE TRANSDUCER                    |
| 6 GAS SUPPLY PRESSURE GAUGE    | 14 GATE VALVE                             |
| 7 INSIDE SOLENOID VALVE        | 15 VACUUM SPHERE                          |
| 8 MANUAL FLOW REGULATING VALVE |   |

Figure 3. Gas Delivery System (Schematic)

gas is delivered to a pressure regulator and then through an on-off solenoid valve to the test area. A manual bleed valve is also provided outside the building test area to permit ready depressurization of the lines. Inside the building the gas passes in turn through a second on-off solenoid valve, a flow regulating manual valve, a suitable choked orifice, and finally a small check valve before entering the test apparatus located within the evacuated reaction vessel. The hot gases exiting from the apparatus pass over water cooled copper coils located within the reaction vessel and the cooled gases exhaust through appropriate piping and valving into the large vacuum sphere again located outside the building. Pressure gauges located in the control panel indicate the gas supply pressure and the controlled pressure preceding the choked orifice. The pressure within the combustor is monitored by a pressure transducer and the vacuum within the reaction vessel is monitored with a gauge.

The flow of gases to the test assembly is controlled in all cases by choked orifices. These orifices are calibrated with nitrogen and, from these data, the flow with other gases is calculated. A cross-check of the calculation procedure is usually made with argon gas. The manufacturer's quoted purity for each of the gases used in the present program is: CO, 99.3%; N<sub>2</sub>, 99.7%; O<sub>2</sub>, 99.6%; and H<sub>2</sub>, 99.9%.

## 2. ARC HEATER OPERATION

The arc heater used in the test program was a Model N-250 heater made by Linde. The power supply was made by American Rectifier, New York.

To ignite the N-250 arc heater, nitrogen flow was initiated and then a potential was applied between the anode and cathode. A one-eighth inch diameter

carbon rod at cathode potential was passed from behind through a port in the cathode into the space between the electrodes drawing the arc from the anode and affixing it to the cathode as the rod was withdrawn once again through the port in the cathode, (see figure 4). The gas-actuated starter is shown in figure 5.

In a normal run-starting sequence, the cooling water to the arc was turned on, the magnetic coil was energized, full nitrogen flow (appropriately divided between arc and combustor with regard to heat and gas composition requirements) was established, the potential was applied between electrodes and the starter mechanism was actuated. Upon arc ignition the fuel and oxidant gases were fed in. The run shut-down was in the reverse order.

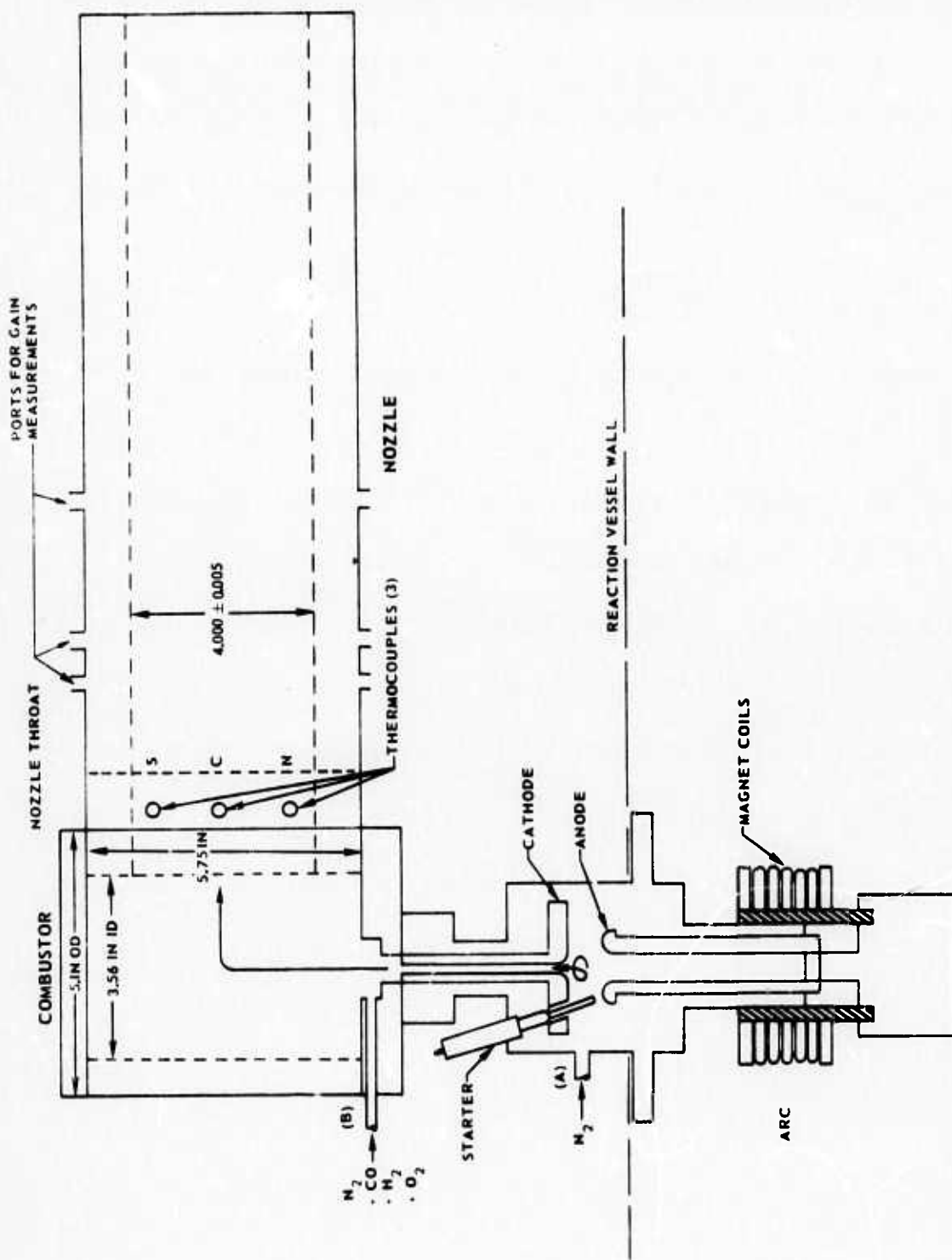


Figure 4. Arc-Combustor-Nozzle Assembly



Figure 5. Arc Starter

## SECTION IV

### EXPERIMENTAL WORK

#### 1. PHASE I

##### a. Design of the Arc-Combustor-Nozzle Assembly

###### (1) General Considerations

The desired operating conditions which the assembly was designed to achieve are listed in Table I. As indicated in Table I a wide range of gas compositions were established for the small-scale gas dynamic laser operating at a stagnation pressure of 40 atm and at a number of stagnation temperatures. In figure 6 is shown a plot of the stagnation temperatures as a function of  $\text{CO}_2$  and  $\text{H}_2\text{O}$  concentrations which result from the combustion of CO and  $\text{H}_2$  with either  $\text{O}_2$  or  $\text{N}_2\text{O}$ . With CO and  $\text{O}_2$  as the principal reactants, approximately 80 kw must be added to the gas stream to achieve some of the desired stagnation temperatures. If reasonable heat losses are considered, then the addition of approximately 200 to 400 kw of thermal power is required to achieve the desired stagnation temperatures. Furthermore, the temperature uniformity within the combustor is exceedingly important in providing meaningful comparisons between theory and experiment. The comparison of theory with experiment also requires that a reasonably shock free gas flow be generated downstream of the nozzle throat to the last port at which gain measurements are made.

The existing UARL mini-rocket GDL was not capable of achieving the desired operating goals, and therefore, was modified at the start of this program. The existing copper combustor had been tested to approximately 35 atm, at which pressure leaks developed because the copper design did not have the requisite structural strength. Also, the proposed test conditions required larger gas

TABLE I

## RUN CONDITIONS

GROUP	RUN	$T_o (^{\circ}\text{K})$	$x_{\text{CO}_2}$	$x_{\text{CO}}$	$x_{\text{H}_2\text{O}}$
1	1	1500	2	0	5
	2	1500	2	30	5
	3	1500	2	60	5
2	4	1500	5	0	2
	5	1500	5	30	2
	6	1500	5	60	2
3	7	1500	6	0	1
	8	1500	6	30	1
	9	1500	6	60	1
4	10	2000	11	0	1
	11	2000	11	30	1
	12	2000	11	60	1
5	13	2000	6	0	6
	14	2000	6	30	6
	15	2000	6	60	6
6	16	2000	4	0	8
	17	2000	4	30	8
	18	2000	4	60	8
7	19	1750	11	0	1
	20	1750	11	30	1
	21	1750	11	60	1
8	22	2000	17	0	1
	23	2000	17	30	1
	24	2000	17	60	1

Other Conditions $A/A^* = 60$  $h_t = .03\text{cm}$  $P_o = 40\text{ atm}$

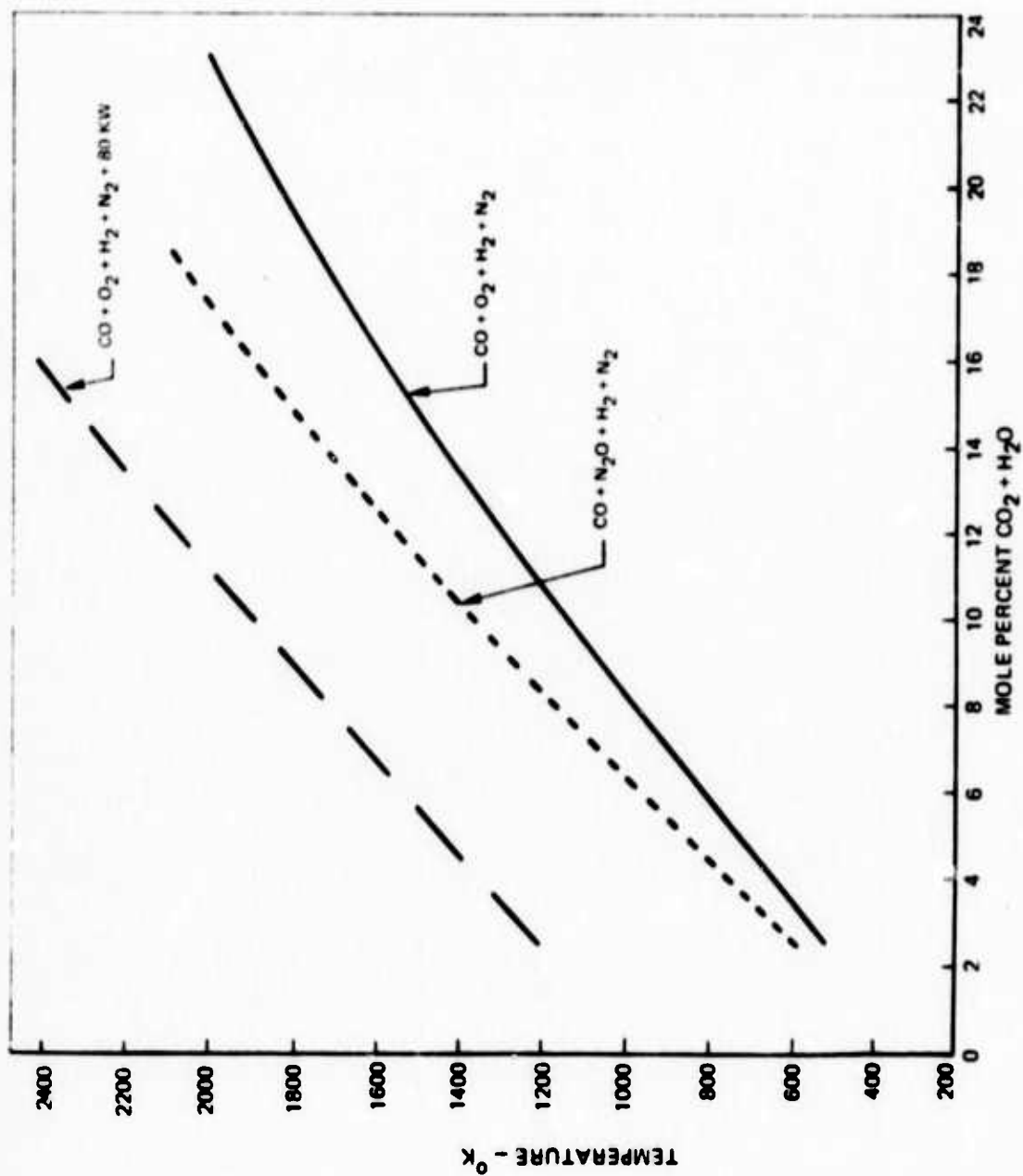


Figure 6. Theoretical Stagnation Temperature Attainable in GDL Minirocket Without Heat Loss

flow rates than had previously been employed, which necessitated replacement of the gas supply lines. Gaseous fuel was considered as the only fuel choice which would allow all of the different conditions to be achieved. Since considerable experience had been obtained in using choked orifices for controlling the gas flows in performing other GDL tests, this same technique, which can readily control gas flows to  $\pm 2$  percent, was chosen for the present study. Some of the early GDL two-dimensional copper nozzle contours were designed with UARL computer programs to provide shock-free flow. These same computer programs were used in the present program.

## (2) Arc-Combustor-Nozzle Design

The modifications which were made to the existing facility to provide the wide ranges of running conditions included a 200-400 kw thermal heat source and a nozzle-combustor design capable of operating at 40 atm while providing uniform gas flow. The following factors were taken into consideration in choosing the thermal heat source: 1) capability of generating the required enthalpy at the desired temperatures 2) potential of varying the enthalpy during a run 3) operation with varying amounts of  $N_2$  and 4) general flexibility. The required enthalpy can be generated by either an arc or a pebble bed heater. (As a result of combustor and nozzle heat losses, exit gas temperatures considerably in excess of  $1200^{\circ}K$  are required). However, only by using an arc can the heater exhaust gas temperature be readily varied during the course of a run. This form of operation is necessary to minimize the number of required runs and yet achieve the desired operating temperatures. Furthermore, the arc is more readily adaptable to operation on the varying amounts of  $N_2$  required

in going from one test point to another. In summary, an arc has more flexibility for this particular program because it can generate the required enthalpies and be readily incorporated into the test apparatus. The arc uses a power supply which can be remotely located. The arc itself has a small volume occupying less than 0.5 cu. ft. of space. In addition, commercial arc units have been operated at pressures well in excess of 40 atm and have delivered the requisite amount of gas enthalpy at temperatures in excess of those required.

Since an arc was chosen as the thermal source, the combustor was designed to mate with the arc in such a manner as to provide a relatively uniform gas temperature at the nozzle throat. To achieve this goal the combustor was designed to have a volume which would provide a relatively large gas residence time. However, the larger the residence time the greater the heat loss; a residence time of approximately 30 m sec was chosen based on previous experience with other types of combustors. The gas emanating from the arc was injected parallel to the nozzle throat in order to dissipate the hot gas plume emanating from the arc. The dissipation of the vortex-stabilized arc gas plume was further enhanced by injecting the reactant gases with a swirl that was opposite to that of the arc heated diluent. Stainless steel was chosen as the material of construction because of its structural properties. Since, in general, the run duration was intended to be less than 30 sec the combustor was only cooled externally so that it could be cooled between successive runs.

The nozzle contour was determined by utilizing the available UARL computer programs. Since the nozzle was to be tested with a variety of gas compositions which corresponded to gas mixtures having slightly differing heat

capacity ratios, the contour was calculated for conditions corresponding to the average gas composition of the test matrix listed in Table I. Because the combustor was made of stainless steel it was thought that the nozzle should be made of a material that had a similar coefficient of expansion to minimize the potential leakage at the combustor-nozzle interface. Furthermore, steady-state calculations indicated that copper might not have the requisite structural strength. However, subsequently it was learned that copper would be acceptable especially for the short run times under consideration. The nozzle was fabricated of stainless steel which resulted in an unanticipated difficulty, namely the nozzle throat changed dimensions during the course of a test. The stagnation temperature uniformity and magnitude upstream of the nozzle throat was to be measured with three equally spaced thermocouples located within the nozzle but just upstream of the nozzle throat.

### (3) Construction of Arc-Combustor-Nozzle Assembly

A diagram of the arc-combustor-nozzle assembly is shown in figure 4. The cylindrical stainless steel combustor is 3.56 inches ID and 5.75 inches long. The internal dimensions of the stainless steel nozzle are  $4.000 \pm 0.005$  inches in width and seventeen inches in length. The nozzle is three inches thick where it joins the combustor (bolted using a copper gasket) and reduces to one and one-quarter inches in thickness shortly downstream of the throat area. The cylindrical arc heater is a Linde arc, Model N-250, which is eleven inches in diameter at the sealing flange and thirteen inches long. Nitrogen is introduced into the arc assembly through four separate nozzles at location (A) so that a swirling flow is set up within the arc. The nitrogen is heated by an arc set

up between a hollow anode and a hollow cathode when the unit is energized. The hot nitrogen plume flows out the hollow cathode toward the combustion chamber. At the entrance of the combustion chamber the hot nitrogen is met by a counter-swirling flow of fuel ( $\text{CO}$  and  $\text{H}_2$ ) and oxidizer ( $\text{O}_2$  or  $\text{N}_2\text{O}$ ) introduced through separate ports at location (B). Combustion begins immediately, is completed within the combustor, and the gaseous product mixture ( $\text{CO}_2$ ,  $\text{H}_2\text{O}$ ,  $\text{N}_2$ , excess  $\text{CO}$ ) then enters the nozzle. The nozzle is made in two halves as shown in figure 7. The internal throat width is four inches and the throat height is 0.12 inches but the height can be adjusted by appropriate selection of shim materials between halves. Ports are provided at five, ten, and twenty-five cm downstream of the throat for gain measurements. The contour of the nozzle was determined through use of computer programs at UARL which include both nonviscous and viscous effects so as to produce shock-free supersonic gas flow. Critical parts of the arc heater, combustor, and nozzle are water cooled. A photograph of the assembly in preparation for installation in the test rig is shown in figure 8.

b. Shake down tests of Assembly in Mini-rocket Facility

(1) Facility Problems

Considerable difficulty was encountered at the beginning of the shakedown tests in isolating problems in the power supply which led to secondary problems within the arc heater. The problems were ultimately resolved to an acceptable degree in conjunction with the power supply manufacturer to enable dependable running of the arc and allow an evaluation of the capability for achieving specified run conditions. This was accomplished principally by

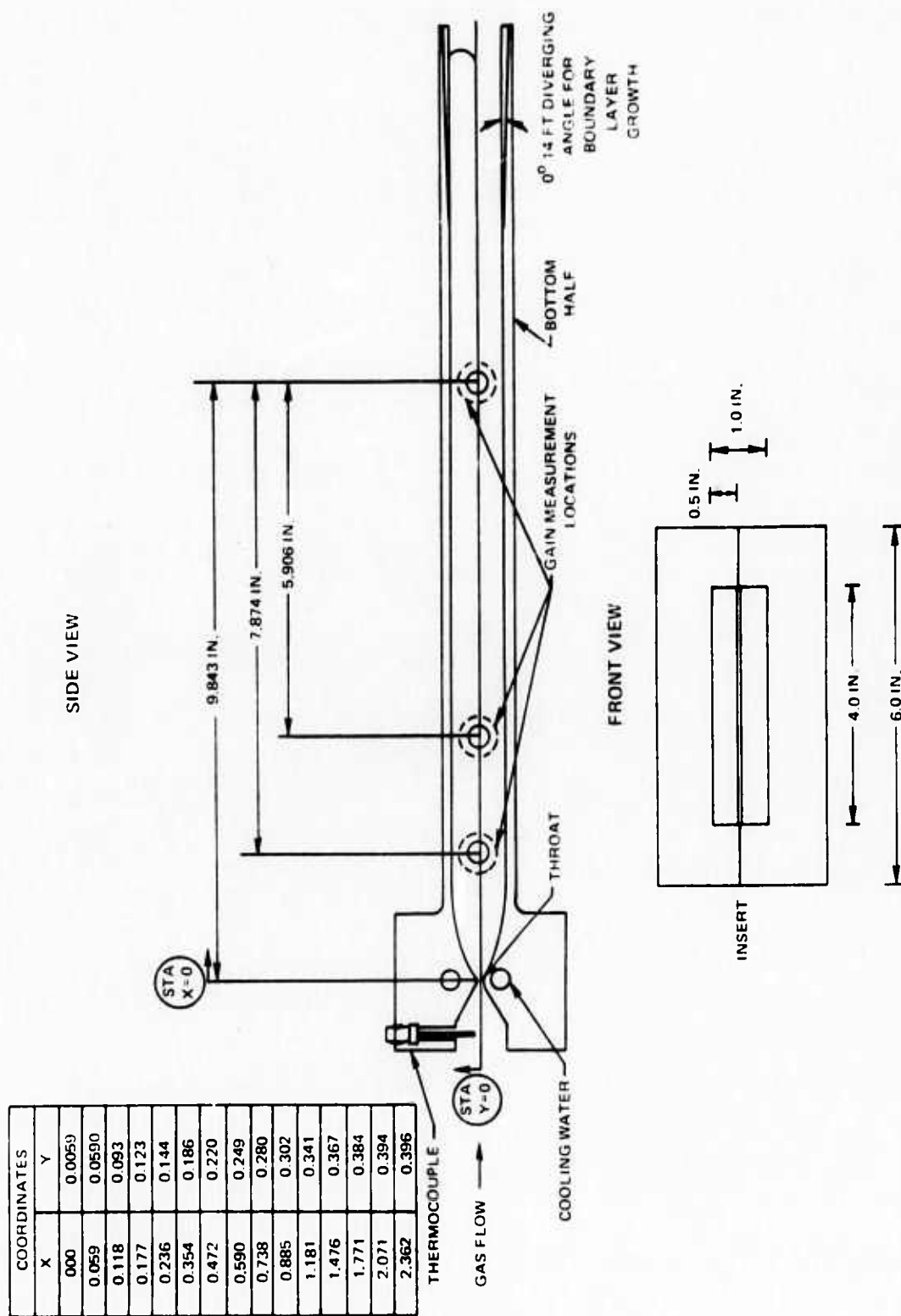


Figure 7. Nozzle Assembly (Schematic)

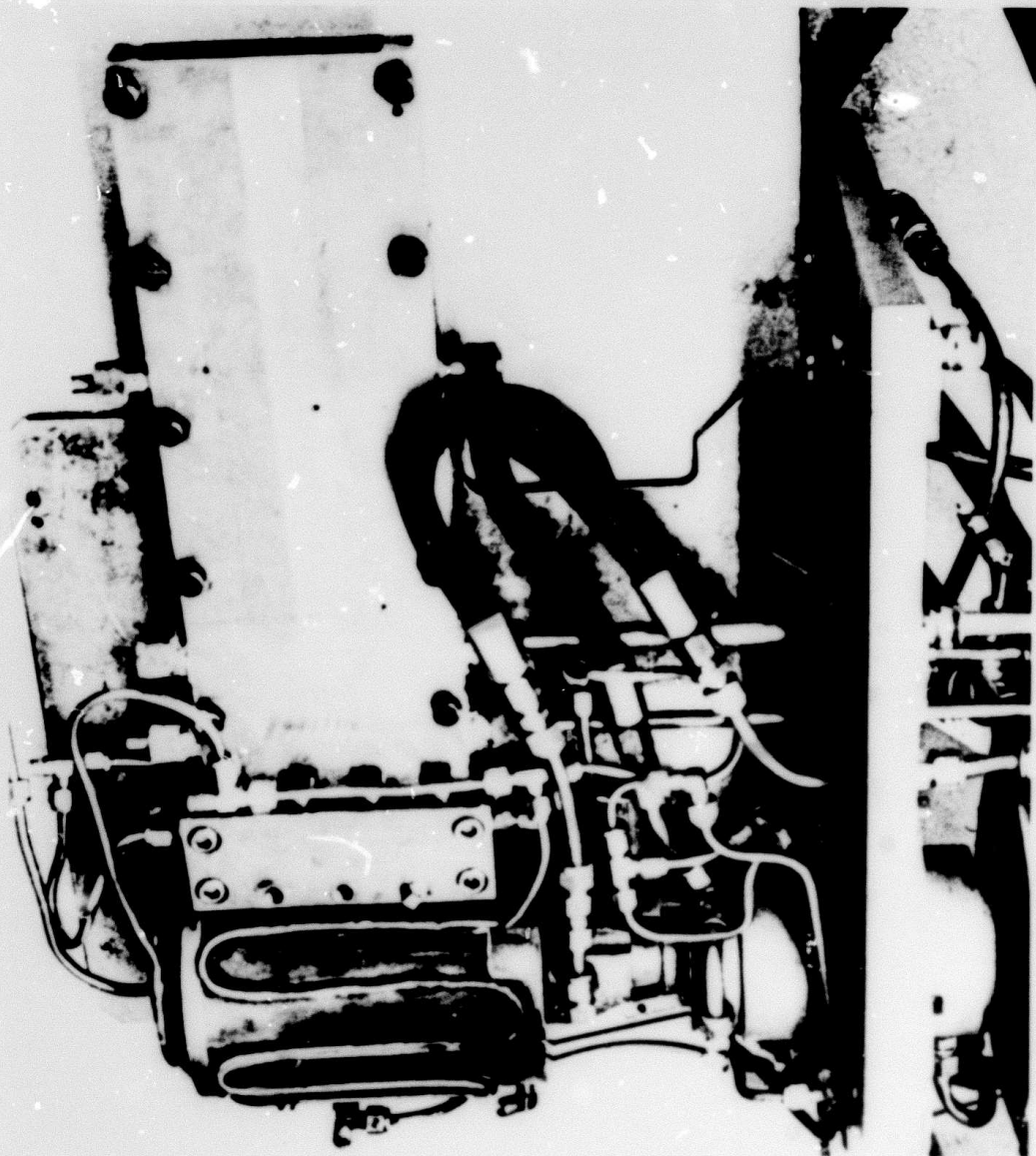


Figure 8. Arc-Combustor-Nozzle Assembly

operating the power supply without output shorting relays and by rewiring and replacing critical power supply components with parts having higher voltage breakdown characteristics. As a consequence of some idiosyncrasies in the power supply, the method of igniting the arc had to be modified to incorporate certain essential procedures. The details of the arc operation are presented in Appendix I.

## (2) Temperature Homogeneity

Three thermocouples were located in the nozzle just upstream of the throat. Their positions are indicated in figure 4. Some initial exploratory runs were made using shielded chromel-alumel thermocouples (steel sheath) which confirmed that temperatures in excess of  $1500^{\circ}\text{K}$  were being achieved. However, these thermocouples burned out at temperatures much above this value. These tests were followed by runs using commercially purchased tungsten/tungsten - 26 percent rhenium thermocouples, both shielded in tantalum and unshielded. These thermocouples lasted only one or two runs when fuel and oxidizer were added, but indicated that design temperatures up to  $2000^{\circ}\text{K}$  were being obtained.

A set of thermocouples having longer lifetimes were made at UARL from platinum/platinum - 13 percent rhodium using a configuration as shown in figure 9. These had a fairly long life time at temperatures up to about  $1600^{\circ}\text{K}$ . These thermocouple configurations were carefully pressure-checked before installation since any pinhole that allowed leakage of hot gases through the thermocouple almost immediately caused disintegration of the epoxy seal on top and catastrophic failure of the thermocouple. If the thermocouple was pressure tight to 900 psig at room temperature, no difficulty was ever experienced during actual

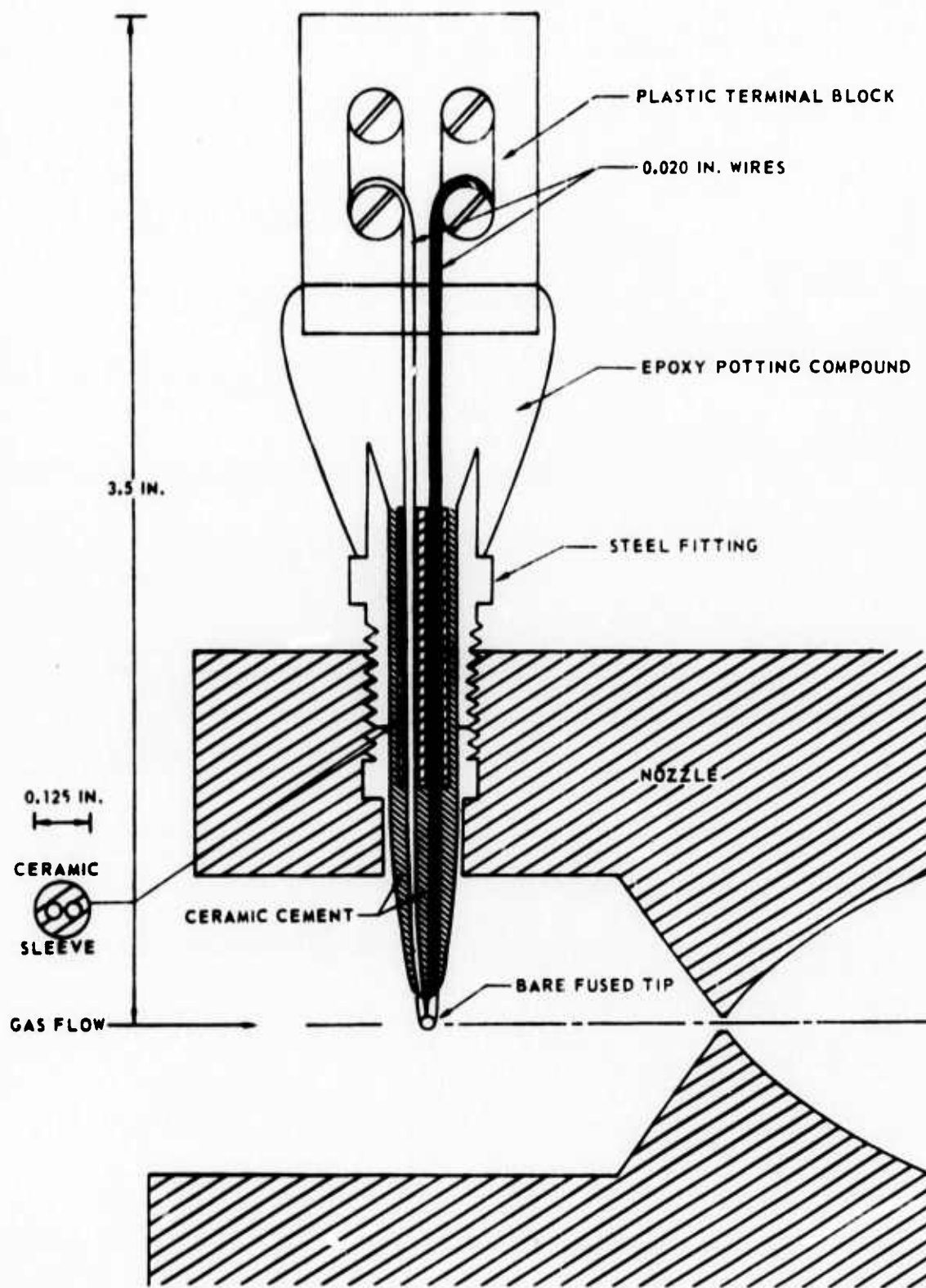


Figure 9. High-Temperature Thermocouple Installation

running. The thermocouple fixture was tested with the platinum/platinum alloy wire because it was more readily available than higher melting point materials. Furthermore, the platinum thermocouples were useful in checking the higher melting point thermocouples to 1700°K; the temperature limit of the platinum thermocouples. By replacing the platinum/platinum rhodium wire with iridium/iridium - 40 percent rhodium wire in the same structure it was found possible to repeatably measure temperatures up to 2100°K. This last thermocouple became the standard tool for measuring temperatures.

A characteristic temperature profile during a run is shown in figure 10. When the arc was ignited ( $N_2$  only) the temperature immediately rose and leveled off. When the fuel and oxidizer were added, the combustion raised the temperature to a higher plateau. By controlling the distribution of nitrogen between the arc and combustor, and by regulating the power output of the arc, fine control of the final temperature was possible.

Temperature data from ten runs are shown in Table II. North, center, and South refer to geographic locations in the nozzle as were signified by N, C, and S in figure 4. The readings are corrected for both radiation and conduction effects as described in Appendix B. The magnitude of the errors in these corrections is estimated at less than 40°K at 2000°K and less than 20°K at 1500°K. On the basis of the data in Table II, the variation in the temperature across the combustor has a maximum value of about 200°K. The values shown in Table II, representing percentages between 4 and 13, are within the maximum allowable deviation of 15 percent. A plot showing several run conditions which were achieved is given in figure 11. For three of the sets of points presented

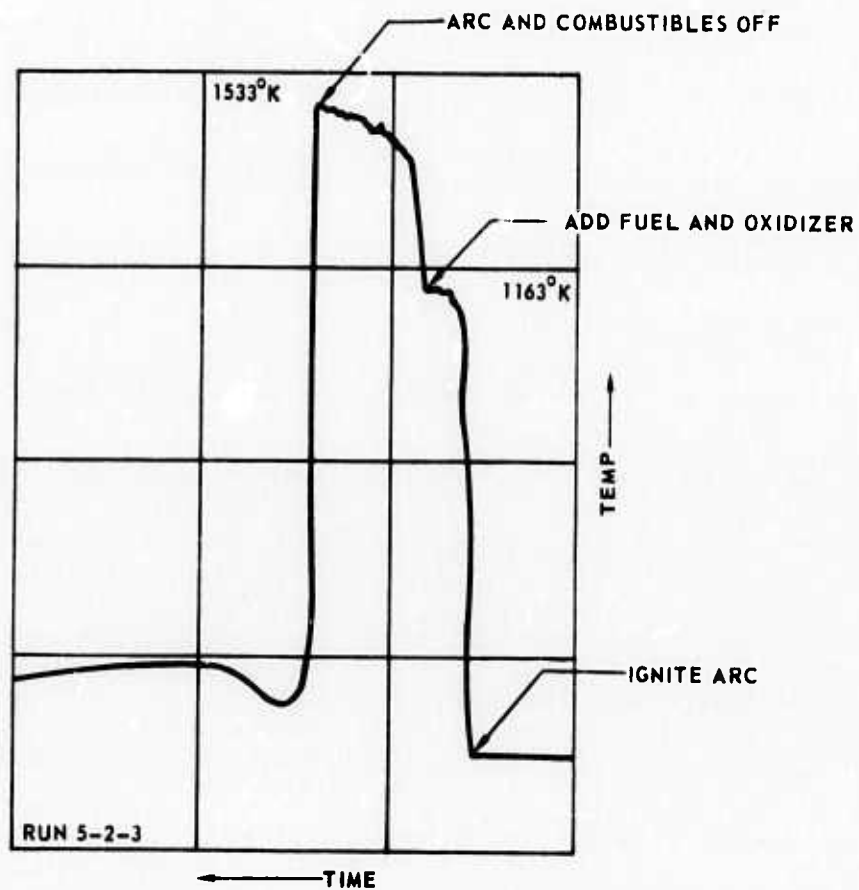


Figure 10. Temperature Profile During a Typical Run

TABLE II  
TEMPERATURE HOMOGENEITY ACROSS NOZZLE

RUN	TOTAL FLOW MOLES/SEC	MOLE %			PRESSURE PSIA	TEMPERATURE-DEG F				ARC POWER KILOWATTS
		CO <sub>2</sub>	H <sub>2</sub> O	N <sub>2</sub>		NORTH	CENTER	SOUTH	AVERAGE	
4-27-6	3.447	2.9	5.4	91.7	680	1310	1315	1360	1330	274
4-28-1	4.48	4.4	8.1	87.5	680	1475	1500	1470	1482	267
4-28-2	4.48	3.97	8.14	87.89	680	1375	1451	1405	1410	305
5-3-1	2.15	3.84	7.86	88.30	632	1829	1725	1780	1778	216
5-6-1	1.967	18.9	1.7	79.40	660	2070	2110	2095	2090	240
5-6-2	1.925	4.47	8.26	87.27	580	1770	1972	1925	1889	238
5-8-1	1.662	3.97	7.9	88.13	640	1995	2230	2260	2160	260
5-8-2	1.619	3.9	8.1	88.0	510	2050	2175	2240	2160	264
5-23-1	3.619	1.82	5.07	93.11	565	1510	1613	1710	1611	326
5-23-2	3.625	2.06	4.97	92.97	685	1580	1780	1780	1713	340
5-24-1	3.628	2.06	5.04	92.9	665	1615	1710	1788	1702	336

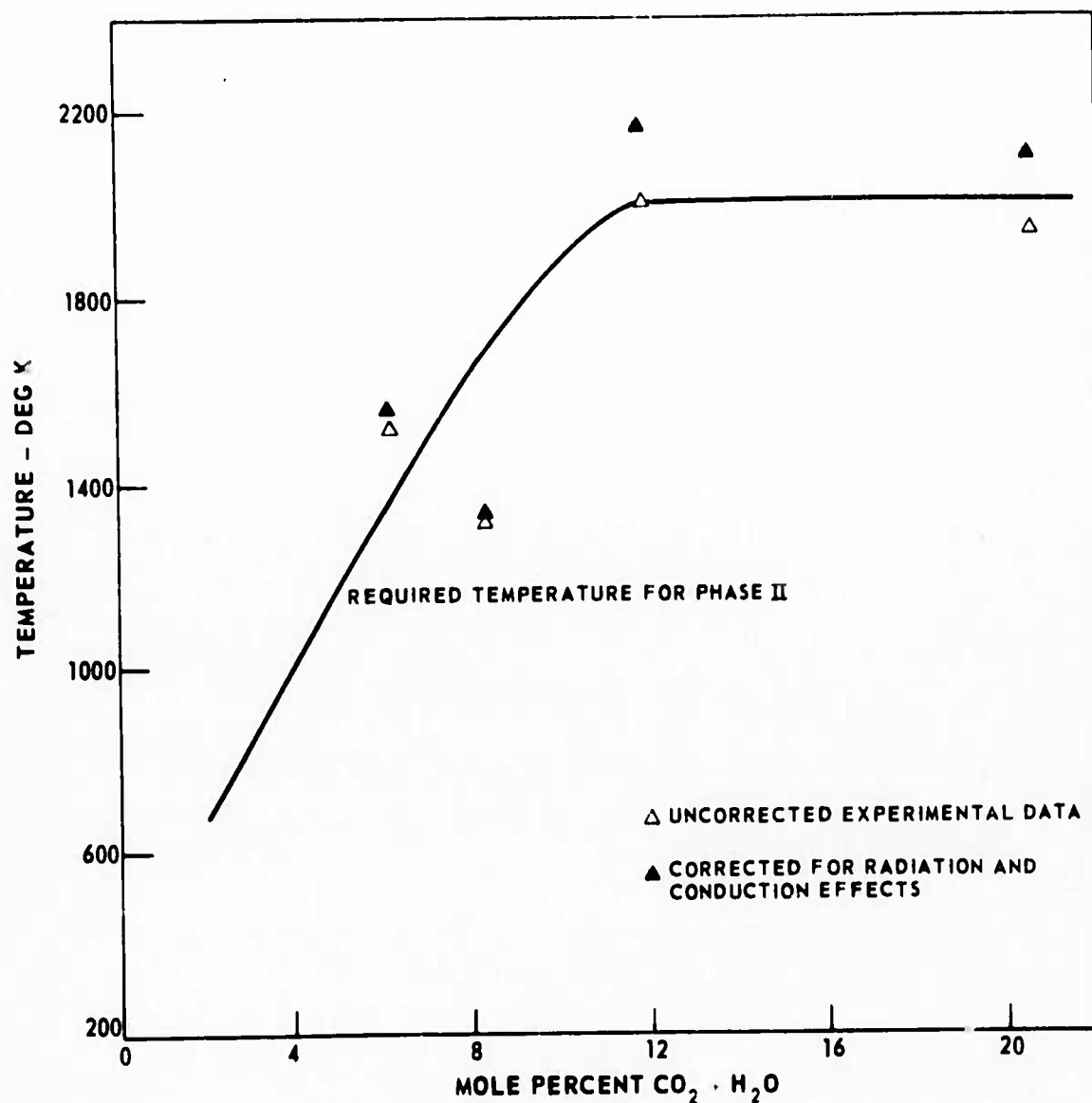


Figure 11. Experimental Stagnation Temperatures with Various Arc Power Settings

in this figure, it can be seen that the stagnation temperatures which were achieved for each gas composition exceeded those required for Phase II. For the fourth point, the arc power setting was too low to achieve the required temperature but ample reserve arc power was still available to reach the required temperatures.

### (3) Pressure Measurements

Figure 12 shows a visicorder tracing of the pressure profile during a test run. (Simultaneous temperature changes are also shown). When the nitrogen flow into the test assembly is initiated, the pressure rises. This has been generally referred to as the cold flow pressure. If this pressure was not consistent with that nominally obtained, it was evident that either leakage or a blockage was present. With ignition of the arc, the pressure rose sharply and then continued to climb. When the fuel and oxidizer entered the system the pressure once more rose sharply until it finally reached a steady state plateau. On the tracing shown, the pressure was read out on two visicorder channels. The first shows the pressure between zero and 670 psia, whereas the second channel is on scale only when the pressure is between 585 (point A) and 670 psia (point B). The greater sensitivity of the latter channel permits a precise measurement of the pressure fluctuations at design pressure. At point C on the tracing the arc current was lowered which served to lower the combustor pressure to 600 psia where it was sustained. At this design condition, the pressure fluctuation was only plus or minus 6.4 psi as shown. This fluctuation is somewhat over 2 percent and consequently well within the allowable limits.

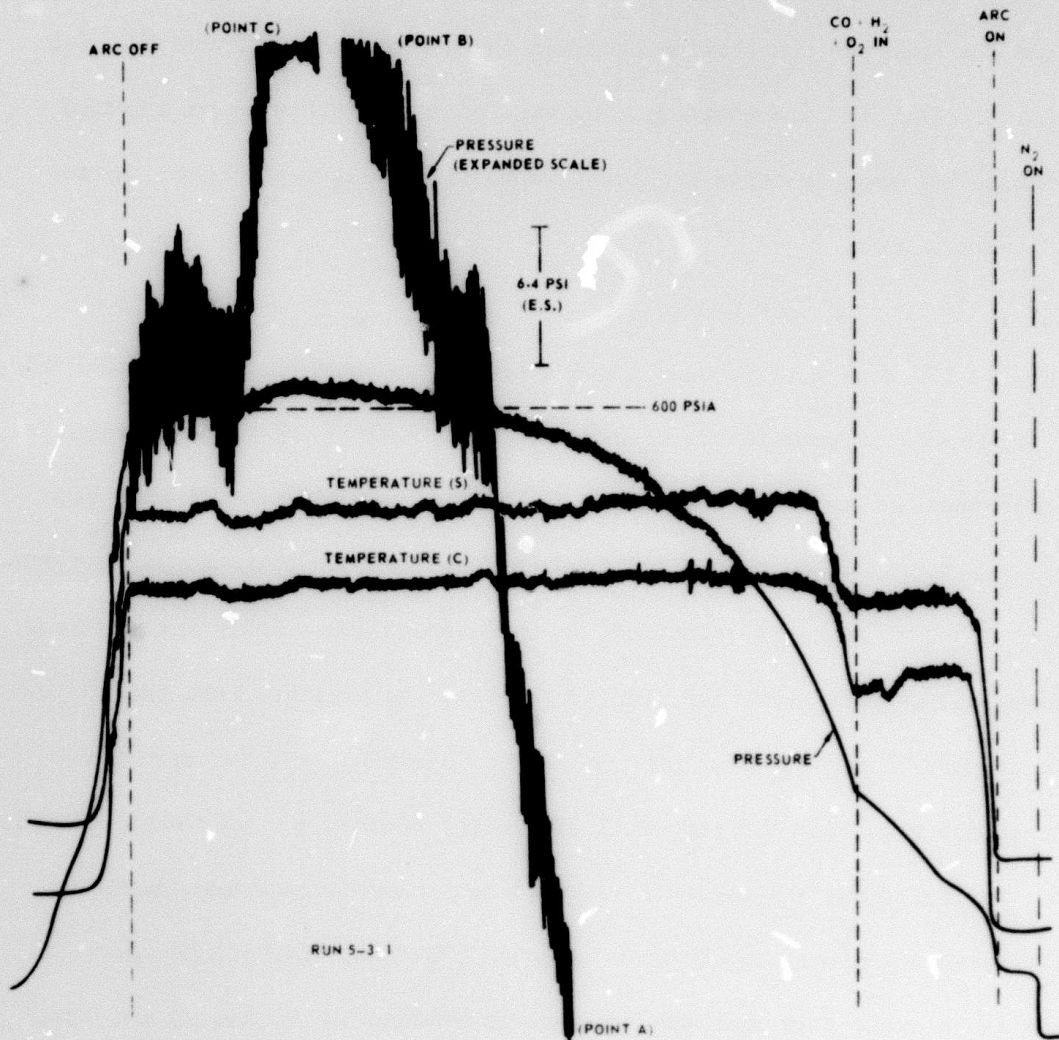


Figure 12. Run Pressure and Temperature Profiles

If the nozzle throat became clogged, this was evident in the observed cold flow pressure and in this event the obstruction was removed. However, during the test sequence, it became evident that the nozzle throat was closing down during each run as the throat became hotter. This was indicated by the very gradual pressure increase which occurred even after the rapid rise in temperature to near steady state had occurred. These results indicated that the temperatures substantially greater than those predicted by the original design analysis were reached by the metal at the throat while the surrounding bulk metal was remaining relatively cool. This resulted in an inward expansion of the metal of the throat and a substantial loss of orifice area. In order to compensate for shrinkage of the throat height at high temperatures, the room temperature throat gap was increased to 0.026 inches using suitable shims. The gap decreased to an apparent gap of 0.012 inches at running temperatures in excess of 1300°K bringing nozzle performance into accord with design gas flow pressure conditions. However, further, more precise, evaluation of the effects of heat transfer on the equilibrium nozzle throat height is still needed to provide a higher degree of confidence in the value of the throat height during test runs. A more detailed discussion of nozzle throat area variations is presented in Appendix III.

#### (4) Gas Composition

Gas compositions and run conditions required by the program are specified in the test matrix in Table I. The gas composition in the combustion chamber is assumed to be that calculated for thermodynamic equilibrium using a standard computer program which uses stagnation temperature, stagnation pressure,

and the relative gas flow rates into the combustor as input data. In this computational procedure, the equilibrium thermodynamic properties of a reacting mixture are obtained by applying a successive approximation procedure to find the simultaneous solution of the standard equations of chemical equilibrium, conservation of (atomic) mass, and conservation of energy for specified values of pressure and either temperature, enthalpy or entropy. The usual thermochemical properties such as temperature and chemical composition, and nozzle flow parameters such as Mach number, velocity, static temperature, static pressure and nozzle area ratio are standard output from this program. Thus by inputting a temperature and relative ratio of inlet gases which is established experimentally, the final gas composition in the combustion chamber is calculated. For a few of the test runs at stoichiometric conditions gas samples were taken and analyzed on a mass spectrometer and gas chromatograph. These analyses indicated that in the cases studied all of the fuel was being fully combusted.

#### (5) Error Analysis

Error analysis techniques used in this study apply standard methods of the type described by Wilson, (reference 10).

The gain,  $g$ , is calculated from the ratio of the experimentally measured intensity,  $I$ , of the probe laser beam when it is passed through the nozzle effluent while running, to the intensity,  $I_0$ , when not running. This calculation is made from the equation

$$I = I_0 e^{gL} \quad (1)$$

where  $L$  is the optical path length. The small signal gain,  $g_o$ , is calculated from the equation

$$g = g_o / (1 + I/I_s) \quad (2)$$

where  $I_s$  is the saturation parameter. Since  $I_o$  in the present experimental work is about  $\frac{1}{2}$  watt/sq cm and  $I_s$  is in the order of 1000 watts/sq cm,  $g$  is essentially equal to  $g_o$  and the experimentally measured gains are essentially the small signal gain values.

Individual errors that affect an overall measurement can be combined to assess the cumulative error in that measurement using the following expression

$$\frac{\Delta Y}{Y} = \left[ \sum_{i=1}^n \left( \frac{\partial \ln F}{\partial \ln X_i} \right)^2 \left( \frac{\Delta X_i}{X_i} \right)^2 \right]^{\frac{1}{2}} \quad (3)$$

Applied to the gain equation,

$$g = \ln(I/I_o)/L \quad (4)$$

this becomes

$$\frac{\Delta g}{g} = \left\{ \left( \frac{\Delta L}{L} \right)^2 + \left( \frac{1}{\ln I/I_o} \right)^2 \left[ \left( \frac{\Delta I}{I} \right)^2 + \left( \frac{\Delta I_o}{I_o} \right)^2 \right] \right\}^{\frac{1}{2}} \quad (5)$$

For  $L = 10.0 \text{ cm} \pm 0.025$

$I = 15.0 \pm 0.030$

$I_o = 14.0 \pm 0.030$

(where  $I$  and  $I_o$  are measured in the same units)

$$\frac{\Delta g}{g} = \left\{ \left( \frac{0.025}{10} \right)^2 + \left( \frac{1}{\ln 15/14} \right)^2 \left[ \left( \frac{0.030}{15} \right)^2 + \left( \frac{0.030}{14} \right)^2 \right] \right\}^{\frac{1}{2}} = 4.33\% \quad (6)$$

and for  $L = 10.0 \text{ cm} \pm 0.025$

$I = 15.4 \pm 0.03$

$I_0 = 15.3 \pm 0.03$

$$\frac{\Delta g}{g} = 27.8\%$$

A summary of the error analyses for representative conditions for this program is shown in figure 13. From this figure it can be seen that the percentage of error is a strong function of the magnitude of the small signal gain, as was evident from the above examples, having a value of about 10 percent at a small signal gain of  $0.4 \text{ percent cm}^{-1}$  and rising rapidly at smaller absolute gain levels.

The error in measured stagnation temperature from thermocouple conduction and radiation effects was discussed in a preceding section. Temperature inhomogeneity, generally about 5 percent but varying to 13 percent, is within the maximum allowable deviation of 15 percent. The stagnation pressure is measured with a transducer (Data Sensors, Santa Monica, California) and is accurate to approximately 1 percent. The composition of the gaseous products is determined in part by the accuracy with which the fuel and oxidizer flow rates are measured. In general, these gas flows are measured to an accuracy of 1 to 2 percent of the individual reading depending upon actual operating conditions. The relative gas flow rates to achieve a particular gas composition are selected from equilibrium data processed to at least four significant figures via the computer program previously described. Errors introduced by this portion of the calculation are negligible compared to the 1 percent accuracy which is achieved in measuring the gas flow rates in the laboratory. Tests have con-

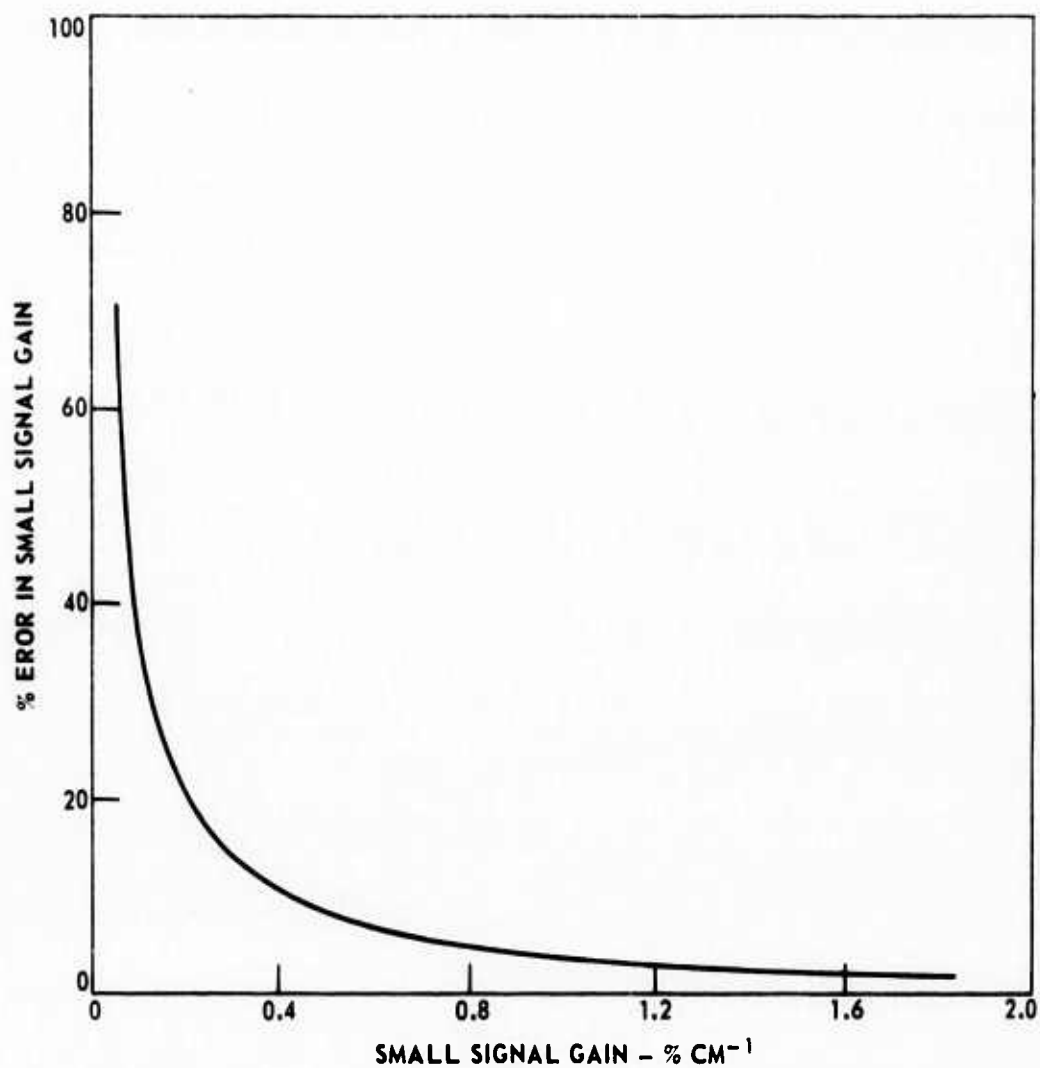


Figure 13. Variation of Error in Gain Measurements with the Magnitude of the Small Signal Gain

sistently shown that the fuel burns completely in the combustor, i.e., below the detection limitations of the mass spectrometer and gas chromatograph, less than 0.05 percent unburned CO and H<sub>2</sub> at stoichiometric conditions. Thus the overall error in the estimated mass fractions of the individual constituents in the combustion chamber is less than 3 percent assuming that the gases are uniformly mixed within the combustor. On line gas analysis across the nozzle exit plane is required to substantiate the degree of mixing. However, because of the long gas residence time within the combustor relatively uniform gas mixing is anticipated. The results of the equilibrium calculations for the conditions listed in Table I are given in Appendix IV.

#### (6) Equipment Reliability

The three items which required frequent servicing were: 1) the arc heater electrodes which deteriorated rapidly under the system operating conditions, (see figures 14 and 15); 2) the nozzle throat (chiefly due to clogging), (c.f. figure 16); and 3) the thermocouples which periodically failed. The first two items required substantial maintenance time after a relatively few runs. The first also involves the expense of new electrodes which were destroyed primarily by the current spikes generated by the arc power supply. The third requires continuous inspection, repair, and replacement. None of these problems with equipment reliability impair the ability to obtain reliable data, but serve rather to slow down the rate at which data can be collected. In addition, some uncertainty still exists as to the time history of the nozzle throat height during a run. This uncertainty is caused by incomplete knowledge of the heat transfer and resultant stresses and deformations near the throat during



Figure 14. Anode Face After 15 Runs



Figure 15. Cathode Face After 30 mins

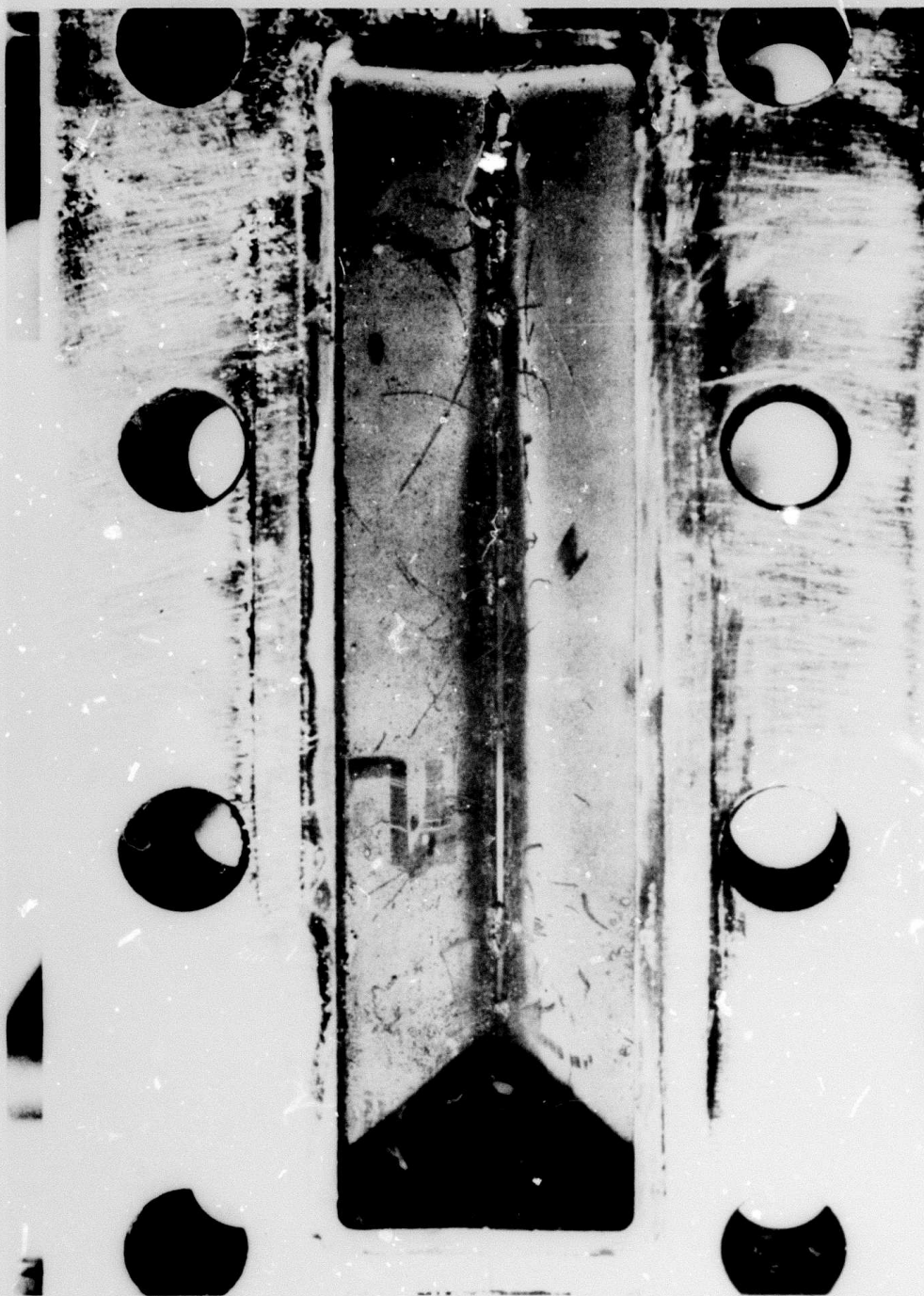


Figure 16. Nozzle Throat After 10 Runs

high temperature operation.

## 2. PHASE II

### a. Gain Measurements

The probe laser used for gain measurements in Phase II was an ordinary CO<sub>2</sub> electric-discharge laser which had been specially modified to improve amplitude stability. This was achieved by enclosing the laser in a constant temperature environment and thermostating the water used for cooling in the laser to control temperature variations to approximately  $\pm 0.1^\circ\text{K}$ . The laser operated on a single frequency, i.e., a single P transition, which was measured using a Perkin-Elmer Model 98 spectrometer. Operation on the exact center of the transition was insured by maximizing the laser output power by changing the mirror separation. The mirror movement was obtained by changing the voltage applied to a piezoelectric crystal attached to the totally reflecting mirror. Two variable apertures located between the laser and nozzle were used to control the optical power and the divergence of the probe beam. These apertures were also used to align the probe laser beam perpendicular to the gas flow to prevent an apparent reduction in gain as described in Appendix V. The apertures were aligned using a HeNe laser beam and some alignment guides.

Since the completion of the Phase I effort consumed more time than was anticipated, an attempt was made to obtain gain data at the three required locations in the nozzle simultaneously rather than at each location in turn, as had been contemplated in the original program plan. To accomplish this, an optical bench was set up utilizing beam splitters and full reflecting mirrors to establish three parallel beams. The optical configuration used is illustrated

in figure 17. An overall view of the laser, optical bench and reaction vessel is shown in figure 18. Although it was possible to align the three beams and to provide adequate power for the measurements, mechanical instabilities in the system reduced measuring sensitivity, and test assembly maintenance procedures caused frequent disruption of the optics and necessitated frequent re-alignment. Primarily, because of the latter problem, the simultaneous gain measurements were abandoned in favor of single beam - single location measurements which could be set up more readily. The single beam was passed through two variable apertures to control the power and divergence of the beam entering the nozzle. The beam intensity leaving the nozzle was detected on a Reeder Detector (6.0 x 6.0 mm window) implemented with a suitably defocusing collecting lens. Since the heated nozzle radiated considerable energy it was necessary to use a beam chopper and a lock-in amplifier (PAR, Model HR-8) to isolate the small signal gain from the background radiation effects. The unmodified mini-rocket facility employed a copper nozzle which did not become hot and therefore beam chopping had not been previously required. Furthermore, the time required to prepare and run the direct combustion GDL was of the order of seconds whereas the arc augmented GDL usually required many minutes for each run. Consequently, with the old facility one could operate the GDL when the probe laser was particularly stable. However, because of the complexity of the arc augmented system all efforts were directed at obtaining arc ignition and the laser stability became of secondary importance.

Some of the gain tracings which were taken are shown in figures 19 and 20. To better delineate the intensity change when the baseline intensity,  $I_0$ , was

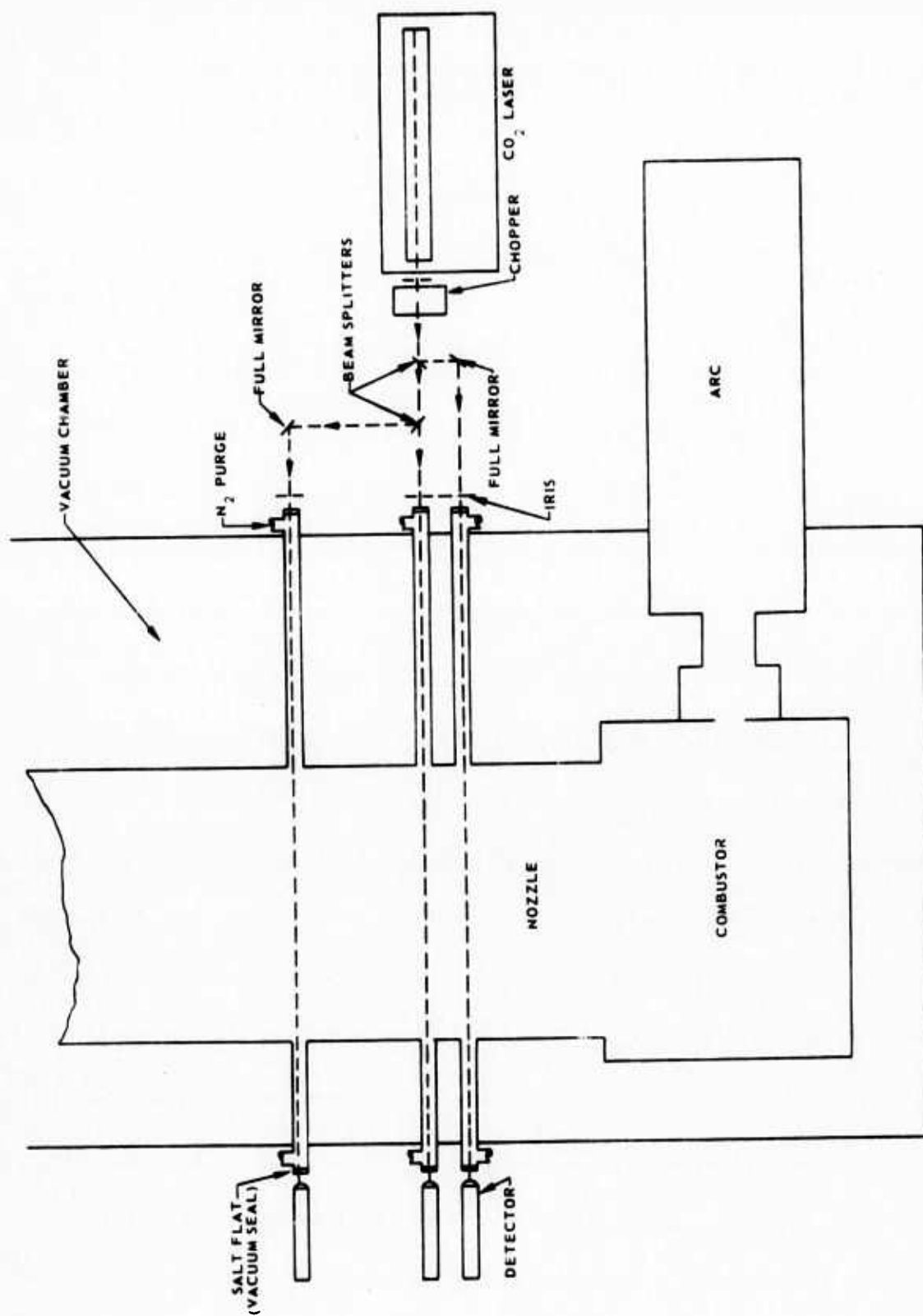


Figure 17. Configuration for Three Simultaneous Gain Measurements (Schematic)

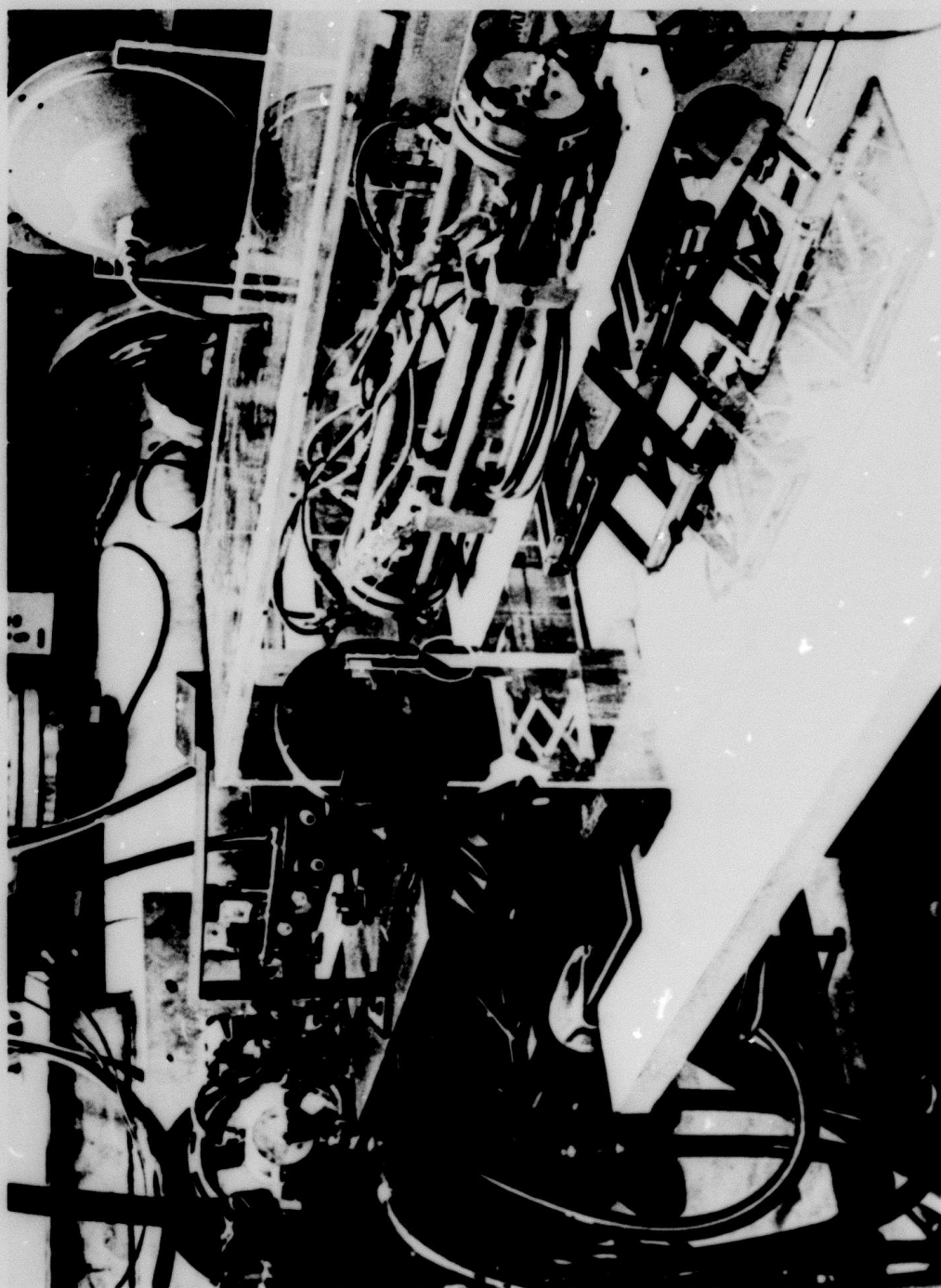
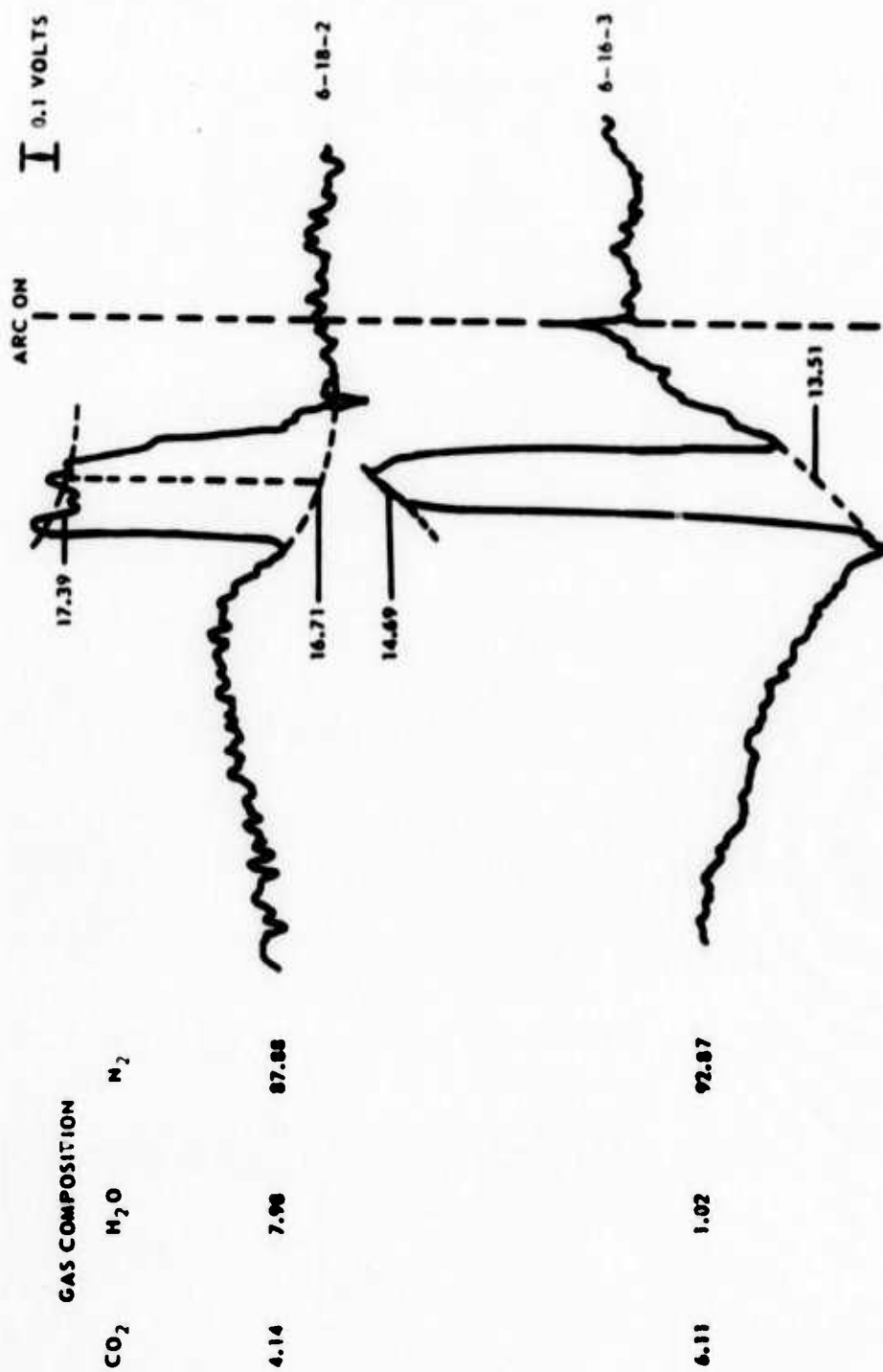


Figure 18. Laser, Optical Bench, and Reaction Vessel Positioned for Gain Measurements



**Figure 19. Gain Tracings, 10 cm Location**

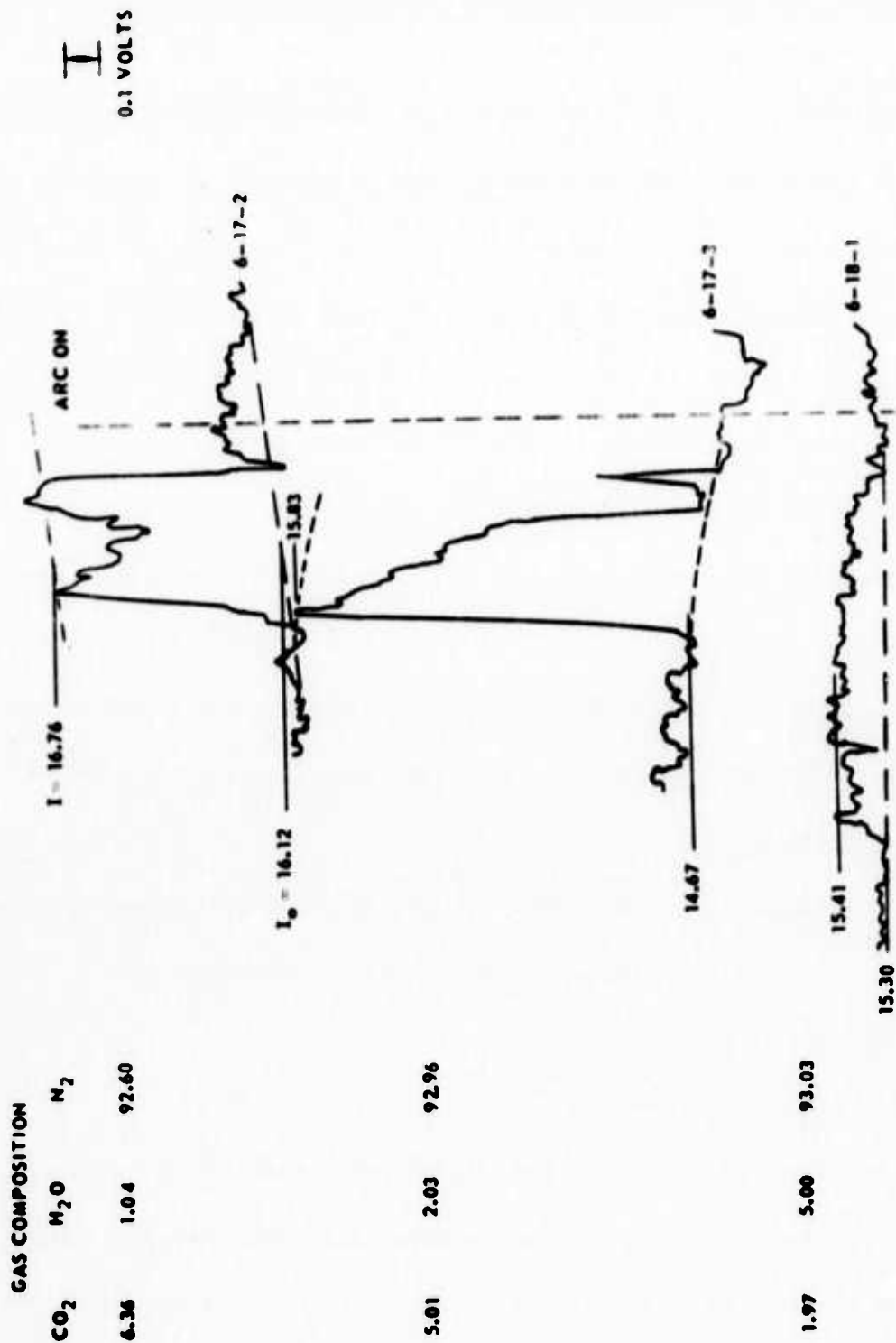


Figure 20. Gain Tracings, 10 cm Location

drifting due to laser drifting, a dashed line has been drawn demarcating the baseline drift and a corresponding parallel line was drawn through the maximum running intensity,  $I$ . The base line drift in figure 19 actually resulted from movement of the nozzle port, as a consequence of the thermal expansion of the nozzle, which resulted in a variation in the transmitted power of the probe laser beam. This situation was rectified by increasing the nozzle port diameter and the drift in the data shown in figure 20 results from a drift in the amplitude of the probe laser.

In figures 19 and 20, the numbers recorded at baseline intensity and at peak running intensity are direct millivolt readings taken off the recorder. Disregarding baseline drift, the noise level generally was about  $\pm 0.03$  mv. Since the intensity values average about 15 mv, the sample error calculations given previously in the error analysis section pertain closely. For example, for run 6-16-3 (figure 19) where  $I = 14.69 \pm 0.03$  mv,  $I_0 = 13.51 \pm 0.03$  mv and  $L = 10 \pm 0.025$  cm, the error is calculated to be 3.42 percent. For run 6-18-1 (figure 20) where  $I = 15.41 \pm 0.030$  mv,  $I_0 = 15.30 \pm 0.030$  mv and  $L = 10 \pm 0.025$  cm, the error is calculated to be 24.0 percent.

#### b. Analysis of Gain Measurements

The small signal gain values  $g_0 = \ln(I/I_0)/L$  calculated for the tracings shown and other similar ones are presented in Table III. The measured values are of the order anticipated. For the first seven runs shown, the nominal gas composition was about 6.0 mole percent  $\text{CO}_2$ , 1 mole percent  $\text{H}_2\text{O}$  and 93 mole percent  $\text{N}_2$ . No excess CO was added in any of these runs. In these runs, temperature and pressure were varied by changing nozzle throat area, by changing

the distribution of  $N_2$  between nozzle and arc heater and by changing the total gas flow. As expected, correlation between run temperature and measured gain is observed (figure 21), although a somewhat less sensitive relationship had been expected from previous work. A single theoretical point supplied by the contracting agency is noted on the figure. This point is not inconsistent with the experimental data points. Combustor pressure varied from 360 to over 750 psia in these test runs but no correlation with measured gain was noted. No correlation with total gas flow was evident as well.

A gaseous composition expected to produce very small gain was utilized for the last run shown in Table III. No difficulty was encountered in making a measurement. Measurement was aided in great part by the simultaneous production of pressure and temperature traces which readily define the time period over which gain may be looked for on the gain trace. This is illustrated in figure 22 where the three simultaneous tracings are shown. The period over which combustion is occurring is easily discerned on the pressure and temperature tracings and is readily related to the gain tracing.

TABLE III  
EXPERIMENTAL GAIN MEASUREMENTS

RUN	TOTAL MOLES/SEC { CO <sub>2</sub> H <sub>2</sub> O N <sub>2</sub>	MOLE %			FSIA	TEMP-°K	I <sub>0</sub>	I	GAIN % cm <sup>-1</sup>
		CO <sub>2</sub>	H <sub>2</sub> O	N <sub>2</sub>					
6-16-1	3.262	6.08	1.01	92.91	360	1358	13.01	13.76	.560
6-16-2	3.262	6.08	1.01	92.91	495	1358	13.45	14.32	.627
6-16-3	3.898	6.11	1.02	92.87	464	1403	13.51	14.69	.637
6-16-4	3.888	5.86	1.02	93.12	426	1223	18.40	18.97	.305
6-17-1	3.931	6.36	1.04	92.60	510	1223	16.98	17.43	.262
6-17-2	3.931	6.36	1.04	92.60	531	1223	16.12	16.76	.389
6-19-1	3.931	6.36	1.04	92.60	750+	1223	18.37	19.05	.370
6-17-3	3.991	5.01	2.03	92.96	592	1403	14.67	15.83	.761
6-20-1	3.991	5.01	2.03	92.96	750+	1223	9.34	9.55	.220
6-18-2	1.667	4.14	7.98	87.88	550	1748	16.71	17.39	.399
6-18-1	3.805	1.97	5.00	93.03	650	1248	15.30	15.41	.072

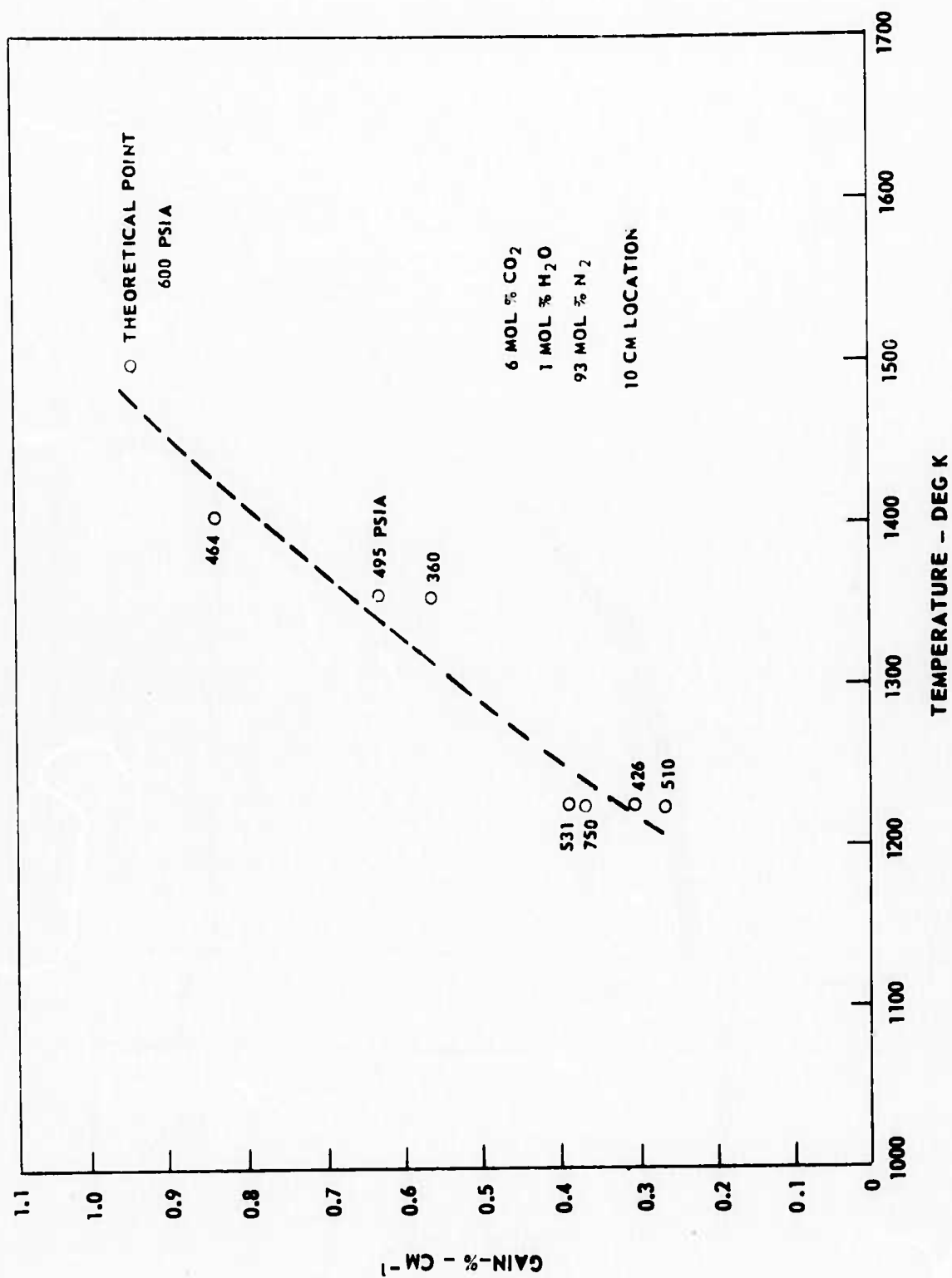


Figure 21. Gain Versus Temperature for Arc-Powered GDL

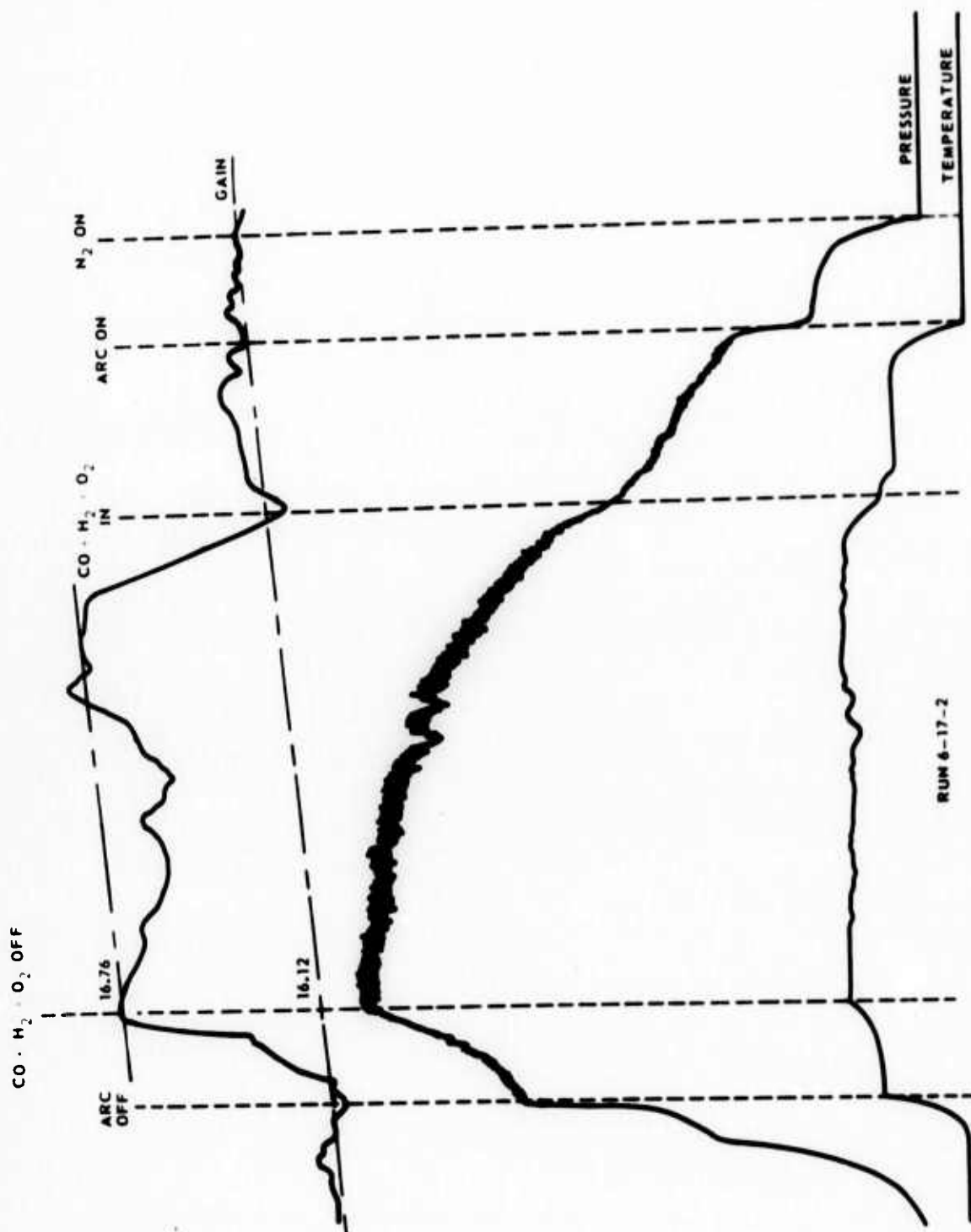


Figure 22. Gain-Pressure-Temperature Tracings

## SECTION V

### CONCLUSIONS AND RECOMMENDATIONS

The following conclusions and recommendations have been reached as a result of the program described herein:

1. The temperature, pressures and gas flow rates desired for measurement of low-signal gain of simulated solid propellant combustion products can be achieved with United's present arc-augmented GDL mini-rocket facility.
2. Optical gain measurement at a single location can be made with accuracies commensurate with those required to distinguish between the laser performance levels of various solid propellant formulations.
3. The probe laser has to be aligned perpendicular to the supersonic gas stream to prevent an apparent reduction in gain that results from the Doppler Effect.
4. Extrapolations of the experimentally measured optical gain in the temperature range from 1200 to 1400 °K are in agreement with theoretical predictions at 1500 °K. The experimental gain data appear to correlate with the measured stagnation temperatures and are relatively insensitive to either gas flow rate or stagnation pressure. However, restrictions in test time precluded the measurement of gain with product gas compositions containing excess CO. Thermodynamic calculations performed for such conditions indicate that the presence of excess CO can significantly reduce the effective water

concentration as a direct consequence of the water-gas equilibrium. Furthermore, significant concentrations of unreacted  $H_2$  are created so that the deactivation of the vibrationally excited  $CO_2$  by  $H_2$  must be accommodated.

5. The optical system used in the present program must be significantly improved if small signal gain measurements are to be made simultaneously at three axial locations in the nozzle. The increase in mechanical stability required for these measurements would also improve the precision of gain measurements at a single axial location. Measurements of gain in the minirocket system should incorporate this more stable gain-measuring system for increased precision.
6. The thermocouple probe designed during the course of this program can be successfully employed in measuring temperature homogeneity within the plenum at temperatures in excess of  $2000^{\circ}K$ . These experimental temperatures can be corrected for both radiation and conduction heat losses to provide a measuring accuracy of approximately  $\pm 4$  percent.
7. The principal source of error in determining the gas concentration within the combustor from thermodynamic calculations results from uncertainties in the value of the stagnation temperature. For a  $200^{\circ}$  change in stagnation temperature at a given nominal value, the nitrogen concentration is not changed at all; however, the calculated concentrations of the other gaseous products may be varied by several percent depending upon the nominal concentration of a particular

constituent.

8. The present configuration of United's arc heater/power supply for the minirocket facility limits the rate at which data can be obtained since the required operating mode leads to rapid electrode deterioration accompanied by plugging of the GDL nozzle by copper from the electrodes. However, additional improvement in the arc-power supply would greatly extend the electrode lifetime and thereby simplify the data acquisition. Qualitative analysis of the nozzle reveals that the copper vaporized from the arc electrodes is deposited in or upstream of nozzle throat or else in the combustor. No copper deposits have been found downstream of the nozzle throat.
9. Some uncertainty as to nozzle throat dimensions during each run exists because of nozzle heating; and resulting stresses and distortion cause a reduction in throat area during runs at temperatures above room temperature. Although the throat height as calculated from gas dynamic measurements appears to stabilize at temperatures above about  $1300^{\circ}\text{K}$ , extensive measurement of the throat height at these temperatures was not made. Future work should include a more complete heat transfer analysis in the region of the nozzle throat and possible redesign of the nozzle to minimize thermal distortion of the throat.
10. The program initiated in the study described in this report should be continued to obtain a more extensive set of experimental small signal gain data at run conditions simulating solid propellant combustion.

## APPENDIX I

### DETAILS OF ARC OPERATION

Conditions to achieve arc ignition using a normal nitrogen flow condition are illustrated in figure 23. This figure shows tracings of voltage and current during successive attempts to achieve ignition by actuating the starter. When the potential was at 900 v, point A, only a small current spike was noted, point  $A_1$ , with no sustained ignition. A potential corresponding to point B (1350 v) produced a higher current spike, point  $B_1$ , but still no sustained ignition. When a potential corresponding to point C (1800 v) was established, a still higher current spike, point  $C_1$ , was obtained this time followed by a sustained ignition as indicated by the sustained current  $D_1$  and the corresponding voltage D. (The current spikes at A, B, and C were actually greater than are indicated in this tracing since these traces were obtained with a relatively slow-response strip chart recorder). The insert added to this figure shows an oscilloscope tracing of the starting spike typified by point C. The current is seen to reach an initial high of about 1600 amp and then taper off over about 150 msec to running current levels. This starting spike causes significant damage to the arc electrodes, but consistently occurred under the improvised conditions necessary to achieve ignition under design nitrogen flow conditions.

From test sequences such as the above, it was hypothesized that an increase in residual magnetization of the saturable reactors of the power supply with each ignition attempt was leading to the successively higher starting potentials

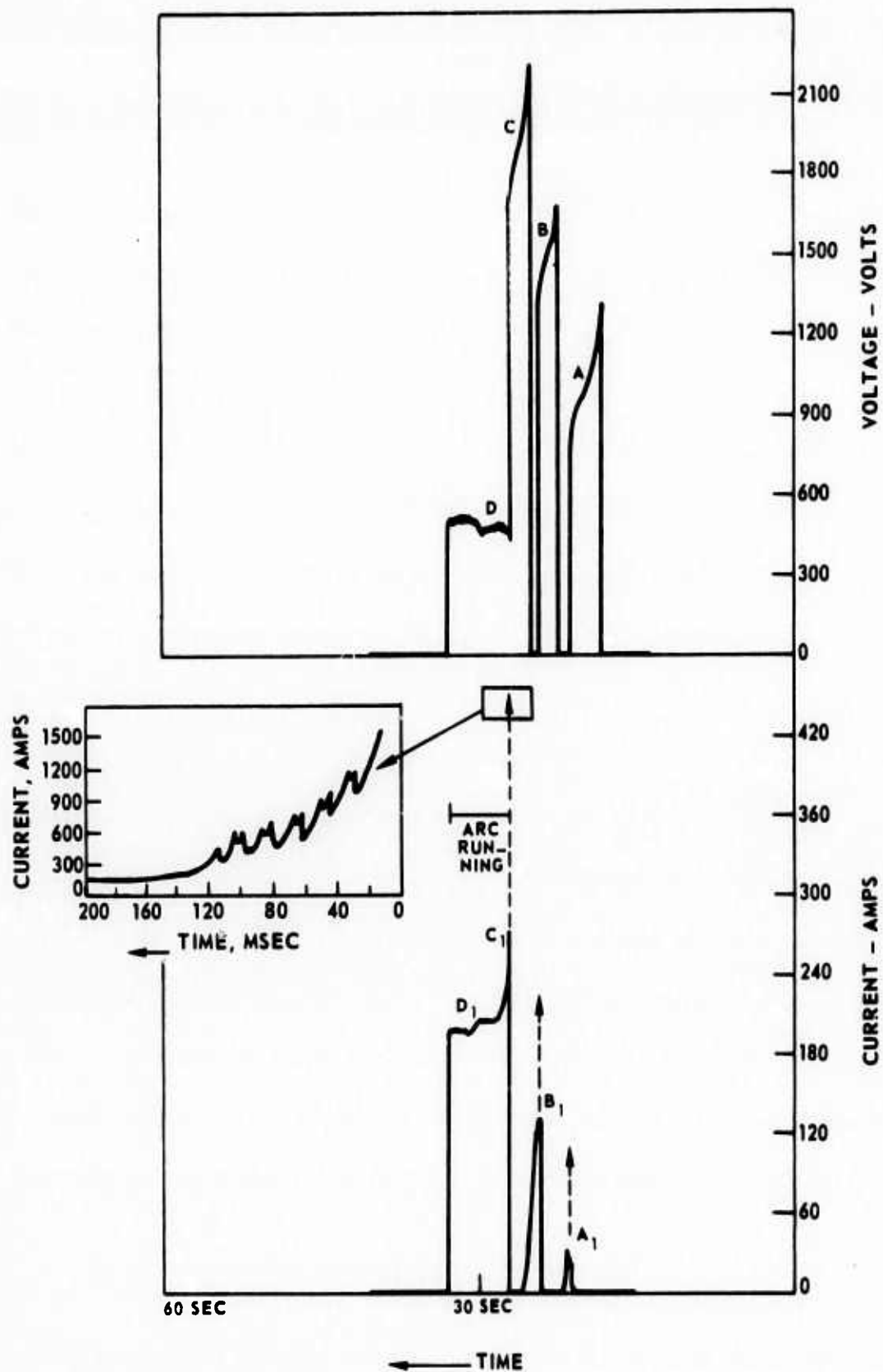


Figure 23. Voltage and Current Traces During Arc Ignition

and currents. The same premagnetization could alternatively be accomplished from the wall control panel using a battery and simple manipulations of the panel meter relay and the saturation current adjust knob. By appropriate premagnetization using the latter technique, it was possible to repeatedly achieve conditions for first try ignitions. However, the current spikes in excess of 1500 amp/cm<sup>2</sup> resulted in the vaporization of portions of the electrodes.

## APPENDIX II

### CONDUCTION AND RADIATION CORRECTIONS TO THERMOCOUPLE READINGS

The derivation of the equations giving the magnitude of the conduction and radiation corrections which have to be made to the thermocouple readings was performed in reference 11 and will not be reproduced herein. Physically the conduction error arise from the conduction of heat away from the thermocouple junction via the thermocouple wire. The radiation error results from the fact that the thermocouple junction radiates heat and if the surrounding walls are not at the same temperature they do not radiate at the same magnitude resulting in a net reduction of the junction temperature. The pertinent equation as derived in reference 11 is

$$T_g = T_w - \bar{\epsilon} \left[ (1 - \alpha_{g,d}) \left( \frac{T_d}{T_w} \right)^4 - (1 - \Sigma_g) \right] - (T_b - T_w) \frac{\psi_m}{1 - \psi_m} \quad (7)$$

where  $T_g$  = Actual gas temperature

$T_w$  = Indicated thermocouple temperature

$T_b$  = Thermocouple support temperature

$T_d$  = Equivalent duct temperature

$\alpha_{g,d}$  = Effective absorptivity of gas for black-body radiation at temperature  $T_d$

$\Sigma_g$  = Effective emissivity of gas

$$\bar{\epsilon} = \frac{\bar{\epsilon}_1 \Sigma_w}{1 + 4 \bar{\epsilon}_1 \Sigma_w \Sigma_g / T_w}$$

$$\bar{\epsilon}_1 = 0.93 \times 10^{-10} T_w^{3.82} \sqrt{\frac{D}{M_1 P}} (1 + 0.2M^2)^{\frac{1}{4}}$$

$\epsilon_w$  = Emissivity of thermocouple wire

$\psi_m = \text{sech}(\eta L/2)$

$$(\eta L)^2 = (\eta_1 L)^2 (1 + 4\beta_1 \epsilon_w / T_g)$$

$$(\eta_1 L)^2 = 1.71 \times 10^{-3} \frac{(DM_p)^{\frac{1}{2}} T^{0.18} (L/D)^2}{k_w (1 + 0.2M^2)^{\frac{1}{4}}}$$

D = Thermocouple wire diameter

M = Free stream Mach number

P = Static pressure

$k_w$  = Thermal conductivity of thermocouple wire

The corrections listed in the text were made using the above equation, however, the evaluation of the equation for particular conditions was greatly facilitated by the use of nomographs also supplied in reference 11. Some error in the magnitude of the correction resulted from estimating the magnitude of certain quantities like the effective temperature of the inside combustor wall and the thermocouple support temperature. Since the absolute magnitude of the corrections were relatively small the error within the correction does not dominate the estimated gas temperature.

# APPENDIX III

## NOZZLE THROAT AREA DURING RUNS

The effective throat area while running can be calculated from experimentally measured gas flow, pressure and temperature data using the formula:

$$A = \frac{W\sqrt{T_0}}{C_D P_0} \left( \frac{R}{M_w} \right)^{\frac{1}{2}} \left[ \gamma \left( \frac{2}{\gamma+1} \right)^{\frac{\gamma+1}{\gamma-1}} \right]^{-\frac{1}{2}} \quad (8)$$

where

A = Nozzle throat area

W = Weight flow

T<sub>0</sub> = Stagnation Temperature

P<sub>0</sub> = Stagnation Pressure

R = Gas Constant

M<sub>w</sub> = Molecular weight

γ = Ratio of the heat capacity at constant pressure to that at constant volume

C<sub>D</sub> = Nozzle discharge coefficient

Since the theoretical magnitude of C<sub>D</sub> approaches 1 at high stagnation pressures and experimental estimates made at room temperature were in agreement with this expectation, C<sub>D</sub> can be neglected. By defining the parameter B as follows:

$$B = \left( \frac{M_w}{R} \right)^{\frac{1}{2}} \left[ \gamma \left( \frac{2}{\gamma+1} \right)^{\frac{\gamma+1}{\gamma-1}} \right]^{-\frac{1}{2}} \quad (9)$$

equation (8) can be simplified to give the following expression:

$$A = \frac{w\sqrt{T_0}}{B P_0} \quad (10)$$

The gas flow parameter, B, varies slightly with temperature and may be calculated with considerable accuracy. Over the temperature range of interest, i.e., room temperature to 2000°K, B varies from 6.318 to 6.164 moles-°K/sec-lb for nitrogen gas.

The effective throat area determined experimentally as a function of temperature for nitrogen gas is shown in figure 24. Above 1000°K, the temperature indicated is the gas temperature as measured just upstream of the throat. The pressure is the final steady state pressure developed over the run. The throat height indicated for room temperature is the throat height measured mechanically when the nozzle was installed. This value correlated well with heights calculated from the gas dynamic equation (10) when cold nitrogen was flowed through the nozzle. It is noted that the throat area appears to decrease with rising temperature up to about 1300°K. It then appears to remain fairly constant as run temperature increases further. At the present time the most likely explanation for this break in the curve appears to be the onset of nucleate boiling in the water cooling passage of the nozzle throat. This phenomenon would serve to maintain a more nearly constant throat temperature though greater amounts of heat are added.

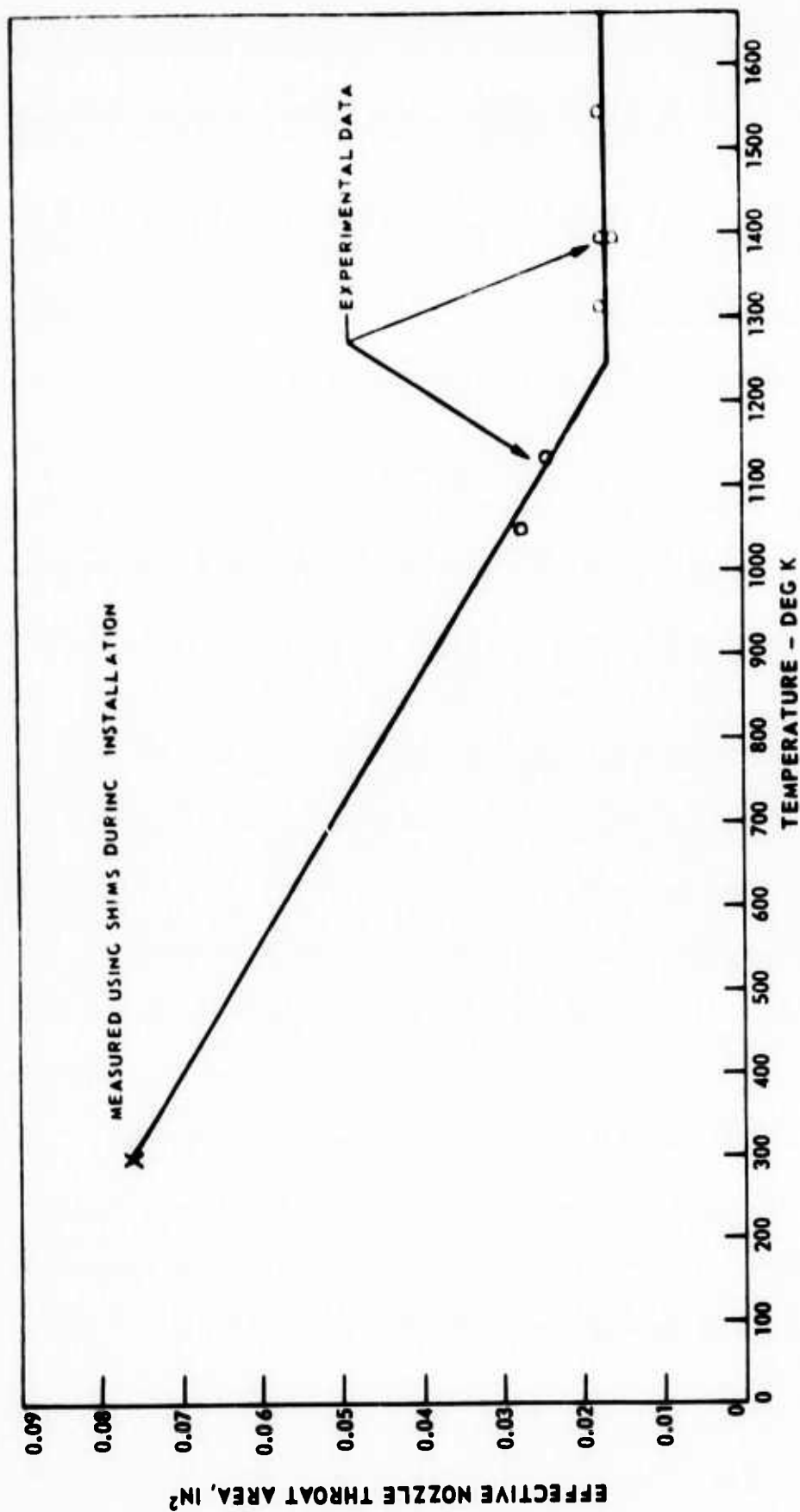


Figure 24. Nozzle Throat Area as a Function of Temperature (Calculated from Gas Flow, Pressure and Temperature Data of --20-72)

#### APPENDIX IV

##### EQUILIBRIUM CALCULATIONS FOR DATA POINTS IN TEST MATRIX

A UARL computer program was used to perform a series of thermodynamic equilibrium calculations for the various gas compositions listed in Table I so that the final gas compositions could be evaluated. The proposed ratio of the individual gas flow rates, stagnation temperature and stagnation pressure were used as input data. In particular, attention was given to the so called water-gas reaction, the equilibrium which exists between  $H_2 + CO_2$  and  $CO + H_2O$ . The effect of this equilibrium for the proposed test points can be observed in figures 25 to 32 by looking at the  $H_2O$  and  $CO_2$  concentrations as a function of the CO concentration. The  $H_2O$  concentration, for example, can vary appreciably as the  $N_2$  is replaced with CO. The data indicates that an appreciable  $H_2$  concentration will be generated whenever substantial amounts of excess CO are present. A summary of the variation in the different concentrations that results from a  $200^\circ$  temperature variation is in the box at the top of each figure.

T = 1500K

PRODUCT VARIATION FOR  $1400 \leq T \leq 1600$

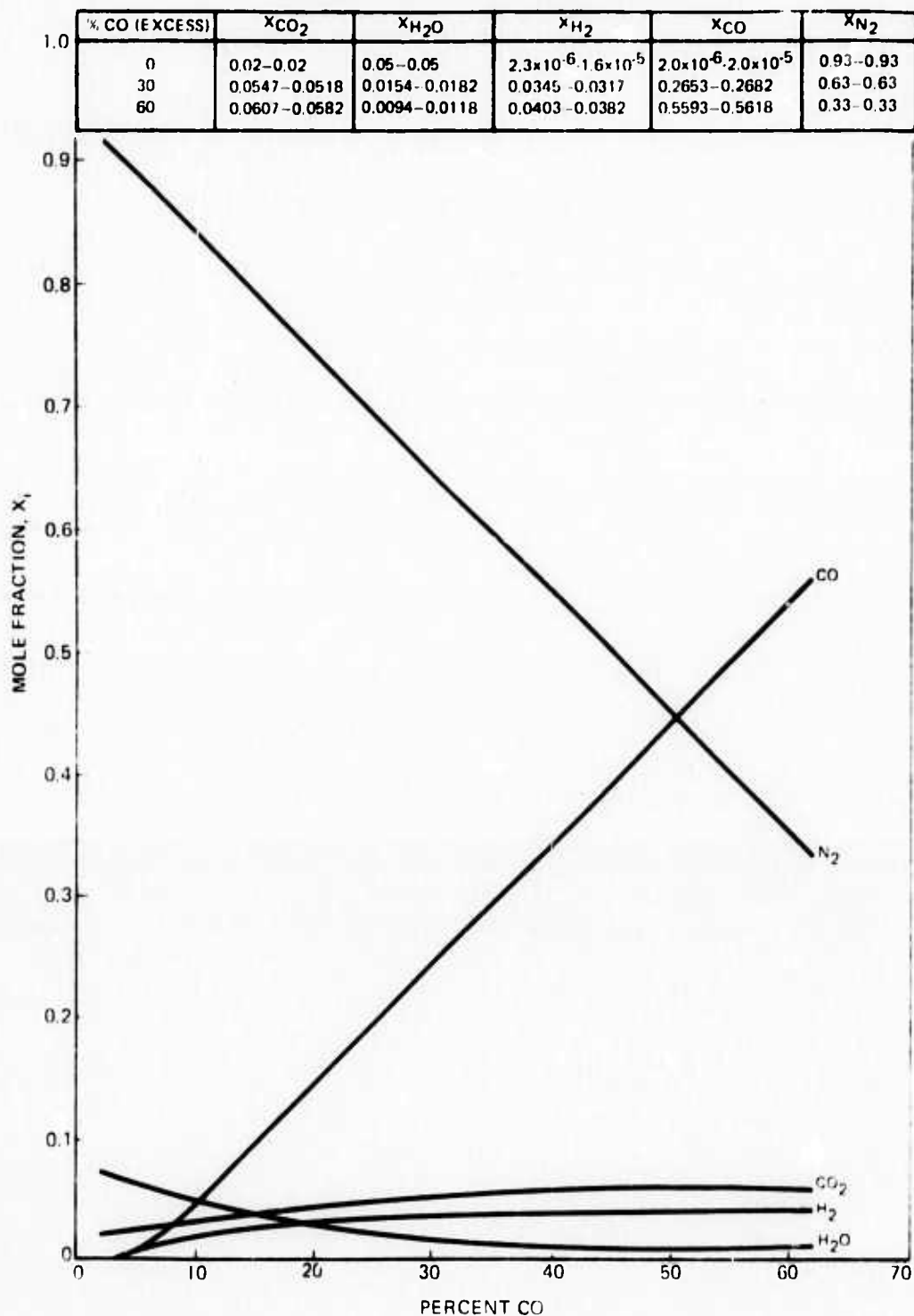


Figure 25. Variations in Combustion Product Composition Corresponding to Run Conditions Listed in Group 1 of Table I

T = 1500K

PRODUCT VARIATION FOR  $1400 \leq T \leq 1600K$

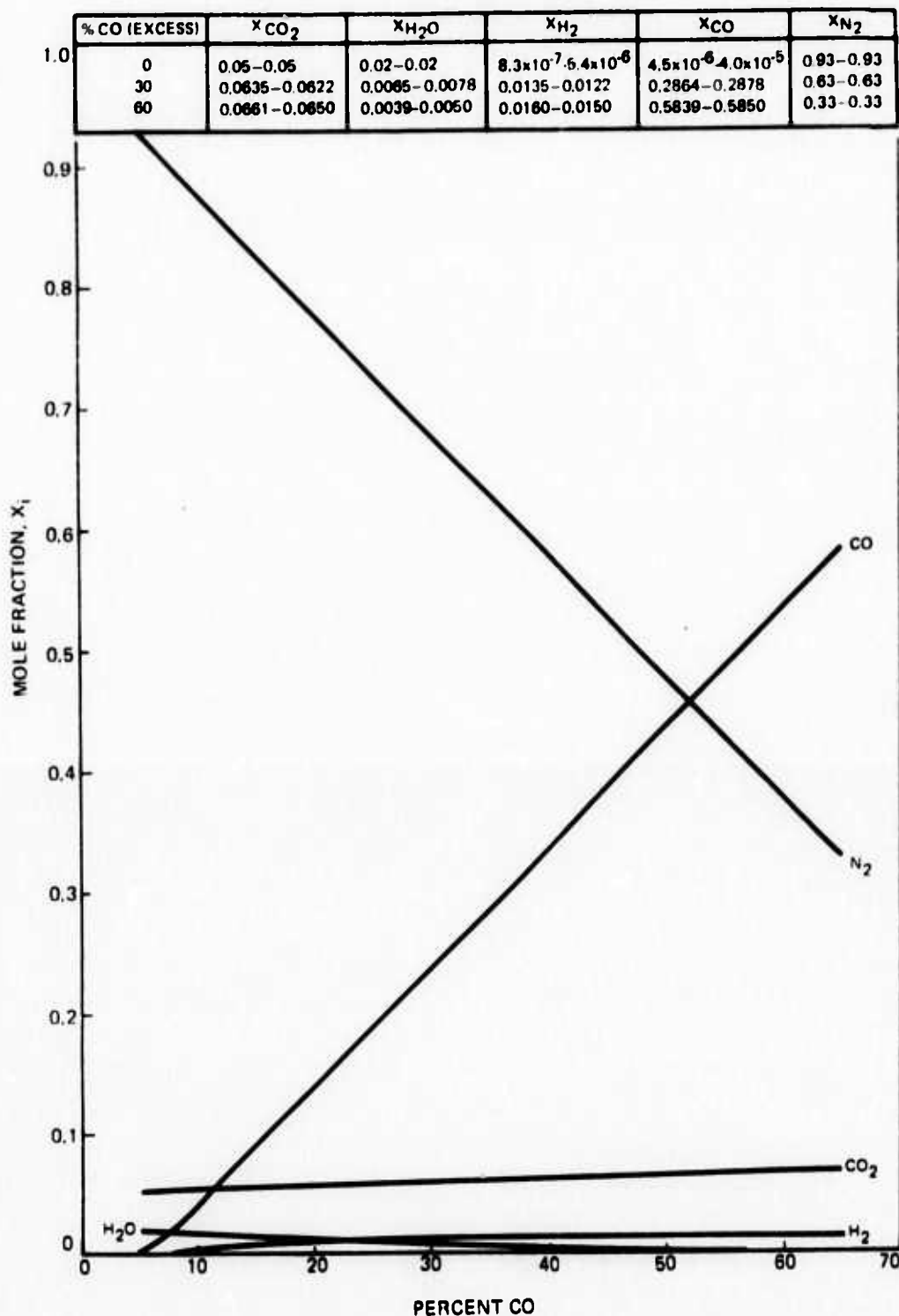


Figure 26. Variations in Combustion Product Composition Corresponding to Run Conditions Listed in Group 2 of Table I

T = 1500K

PRODUCT VARIATION FOR  $1400 \leq T \leq 1600K$

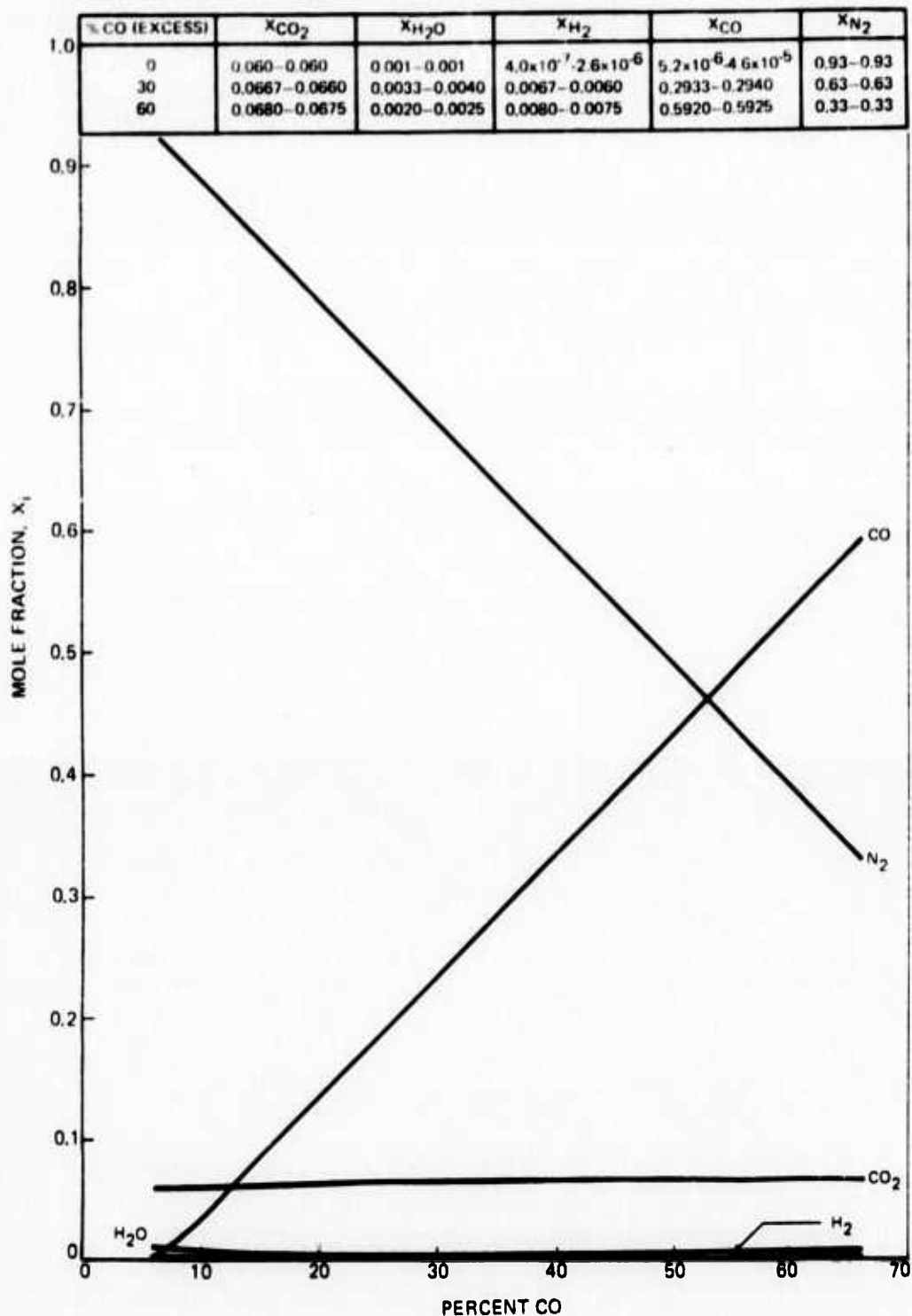


Figure 27. Variations in Combustion Product Composition Corresponding to Run Conditions Listed in Group 3 of Table I

T = 2000K

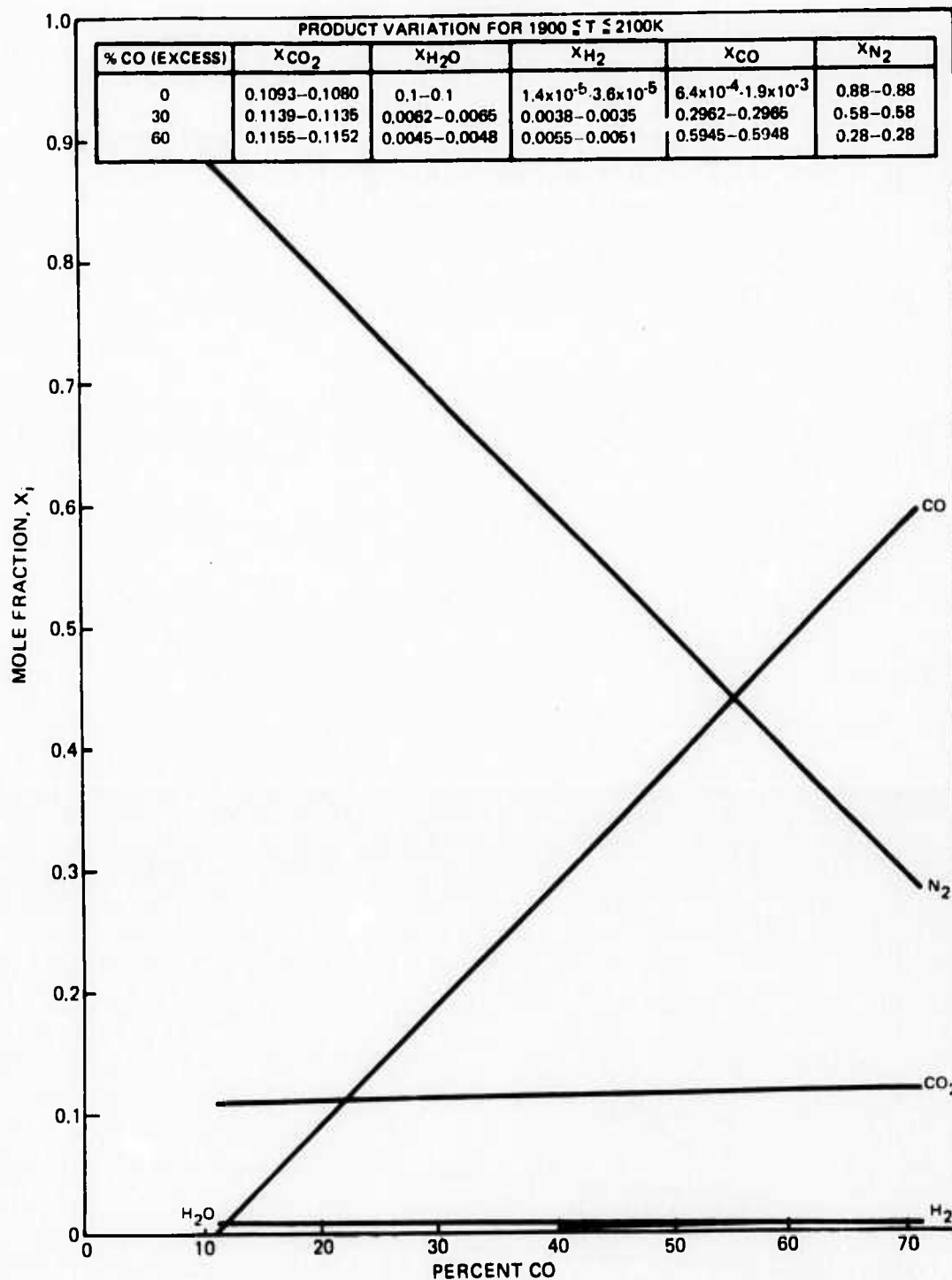


Figure 28. Variations in Combustion Product Composition Corresponding to Run Conditions Listed in Group 4 of Table I

T = 2000K

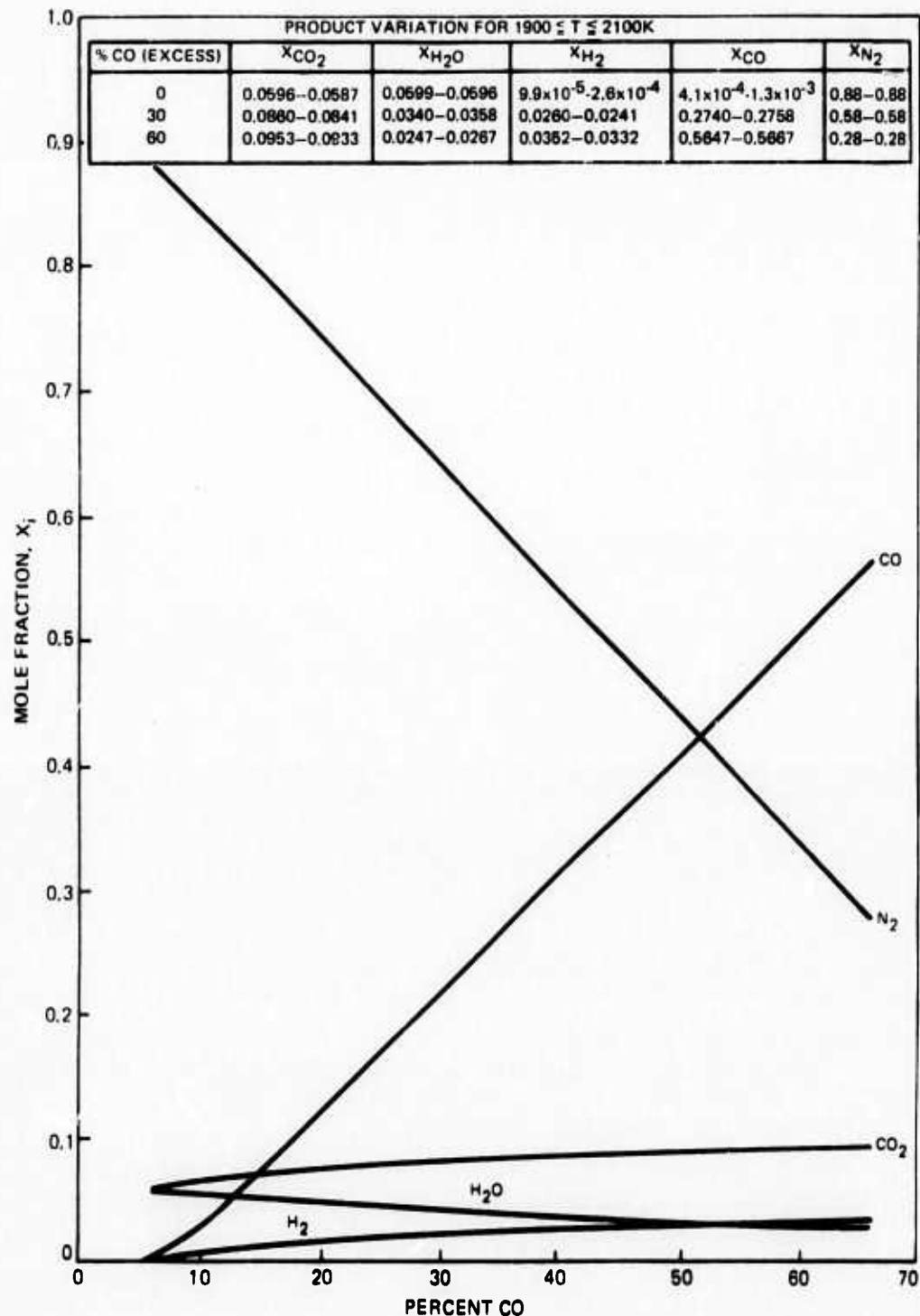


Figure 29. Variations in Combustion Product Composition Corresponding to Run Conditions Listed in Group 5 of Table I

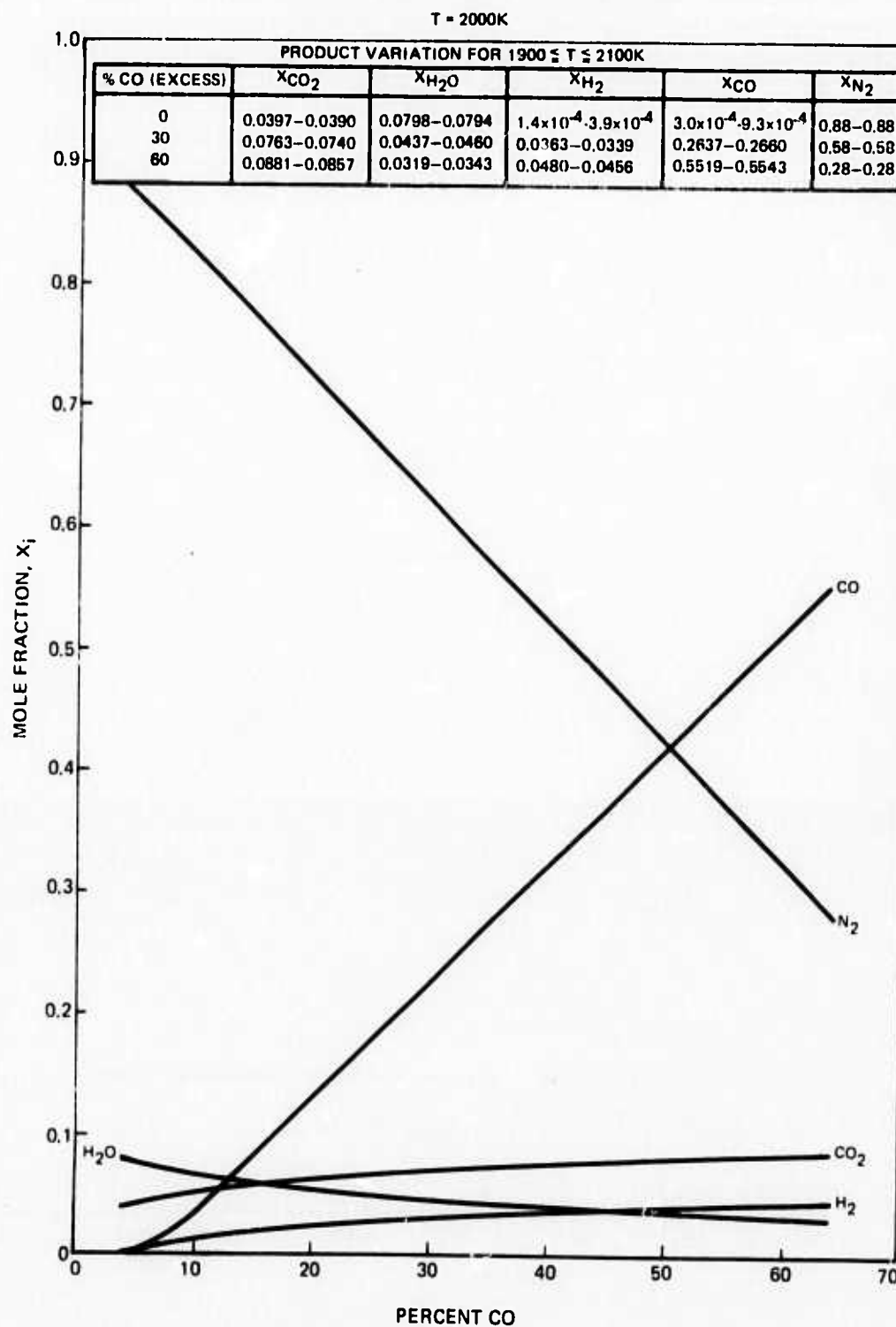


Figure 30. Variations in Combustion Product Composition Corresponding to Run Conditions Listed in Group 6 of Table I

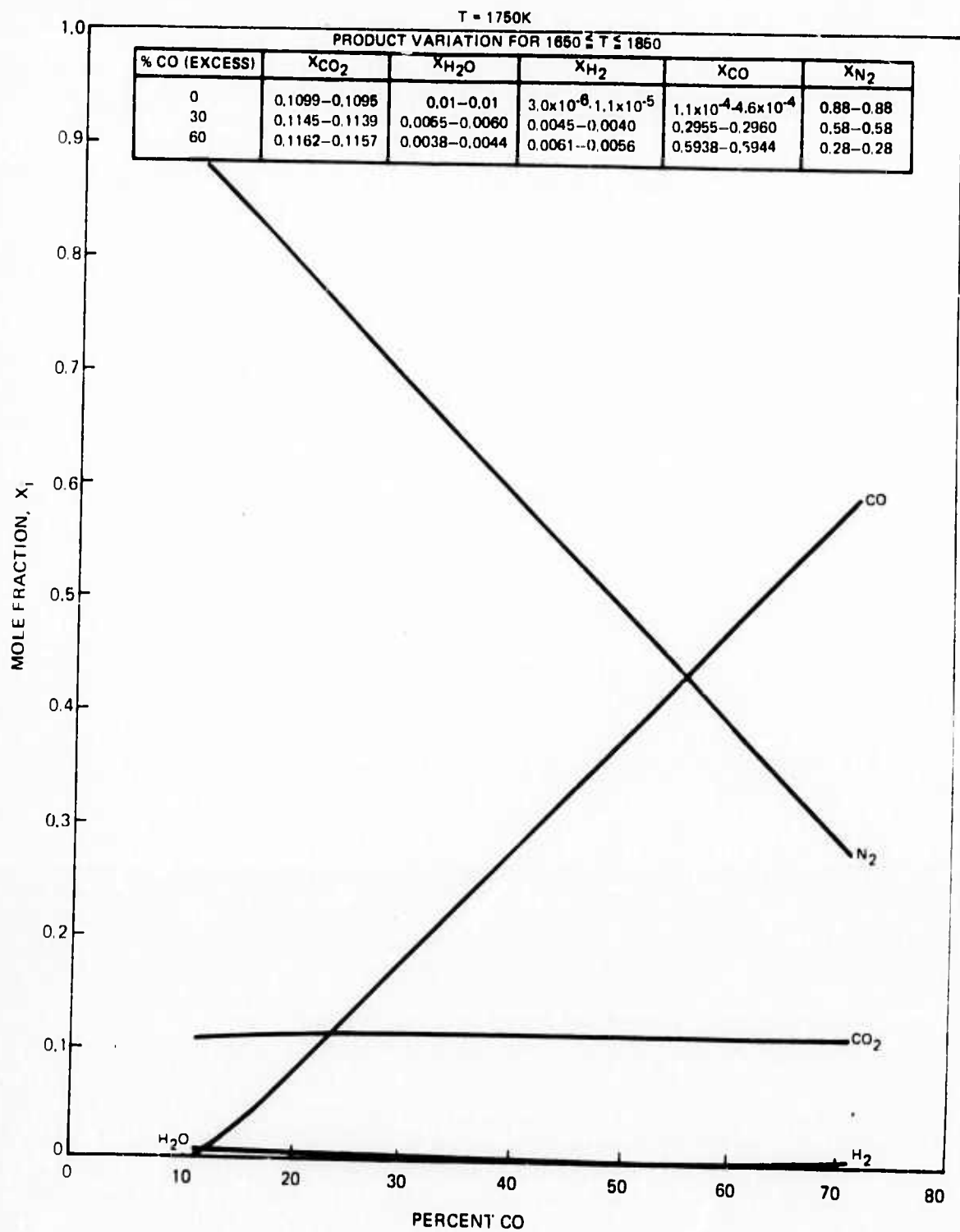


Figure 31. Variations in Combustion Product Composition Corresponding to Run Conditions Listed in Group 7 of Table I

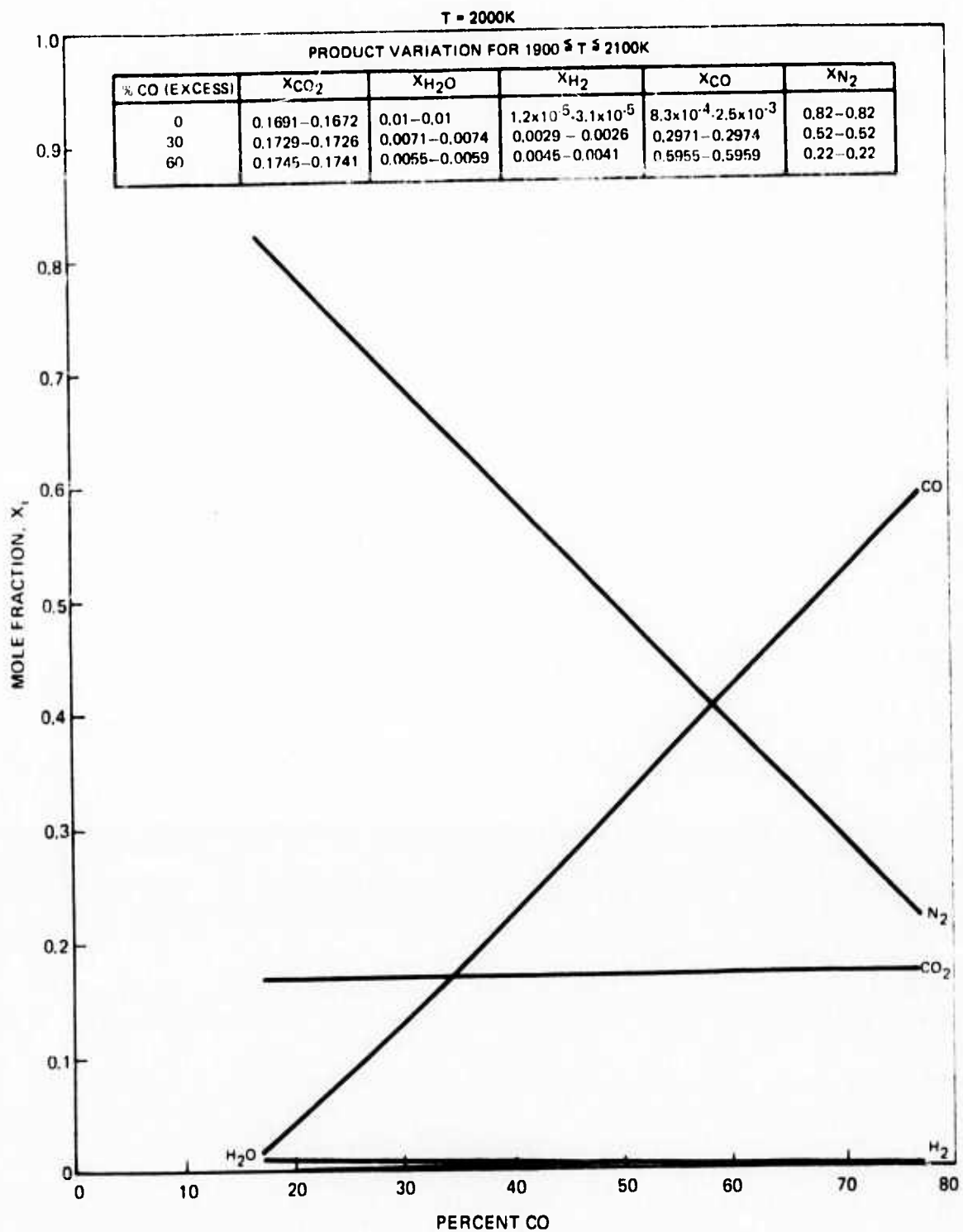


Figure 32. Variations in Combustion Product Composition Corresponding to Run Conditions Listed in Group 8 of Table I

## APPENDIX V

### APPARENT GAIN REDUCTIONS RESULTING FROM THE DOPPLER EFFECT

The importance of aligning the probe laser perpendicular to the supersonic gas stream results from the fact that the gas molecules can sense an effective frequency shift which reduces the measured gain. This frequency shift results from the Doppler effect wherein the bulk velocity of the gas molecules with respect to the probe laser beam direction can cause a relative shift in the frequency distribution of the molecular population. The magnitude of this effect can be calculated from the Doppler equation which is discussed in many references (reference 12).

$$f = f_s \sqrt{\frac{c + V_r}{c - V_r}} \quad (11)$$

where

$f$  = observed frequency

$f_s$  = frequency of stationary source

$V_r$  = velocity of source relative to observer

$c$  = speed of light

By expanding the above equation as a power of  $V_r/c$  and eliminating all powers of  $V_r/c$  greater than 1, the following familiar expression is obtained:

$$\Delta f/f \approx V_r/c \quad (12)$$

In the above equation  $f$  can be considered to be the vibrational frequency of the carbon dioxide molecule and is given by the expression

$$f = c/\lambda \quad (13)$$

where  $\lambda$  is the wavelength and for  $\text{CO}_2$  is equal to  $10.6 \times 10^{-4}$  cm. Furthermore,  $V_r$  is the relative velocity of the gas molecules with respect to the direction of the probe laser beam or

$$V_r = V \cos \theta \quad (14)$$

where  $V$  is the average gas velocity and  $\theta$  is the angle between the bulk gas velocity and probe laser beam. Combining equations (12), (13) and (14) gives

$$\Delta f = V/\lambda \cos \theta \quad (15)$$

Assuming some hypothetical GDL conditions,  $v = 1 \times 10^5$  cm/sec and  $\theta = 80^\circ$ , (a  $10^\circ$  misalignment) gives  $\Delta f = 16.4 \times 10^6$  cps.

An estimate of reduction in gain which results from a frequency shift of  $16.4 \times 10^6$  cps can be estimated from the curve in figure 33. The data in this figure represents the variation in gain with frequency which results from inhomogeneous line broadening, which is calculated by considering the distribution of molecular velocities and applying the same Doppler expression as was used herein with the bulk gas velocity resulting from the supersonic gas expansion. The curve in the figure is only applicable at very low gas pressures where pressure broadening is negligible. If pressure broadening is considered the linewidth becomes larger, and the rate of gain variation with frequency becomes smaller. However, for the sample case which has been chosen it can be seen that a  $16.4 \times 10^6$  cps shift in frequency caused by a  $10^\circ$  misalignment

NOTE: PRESSURE BROADENING NEGLECTED

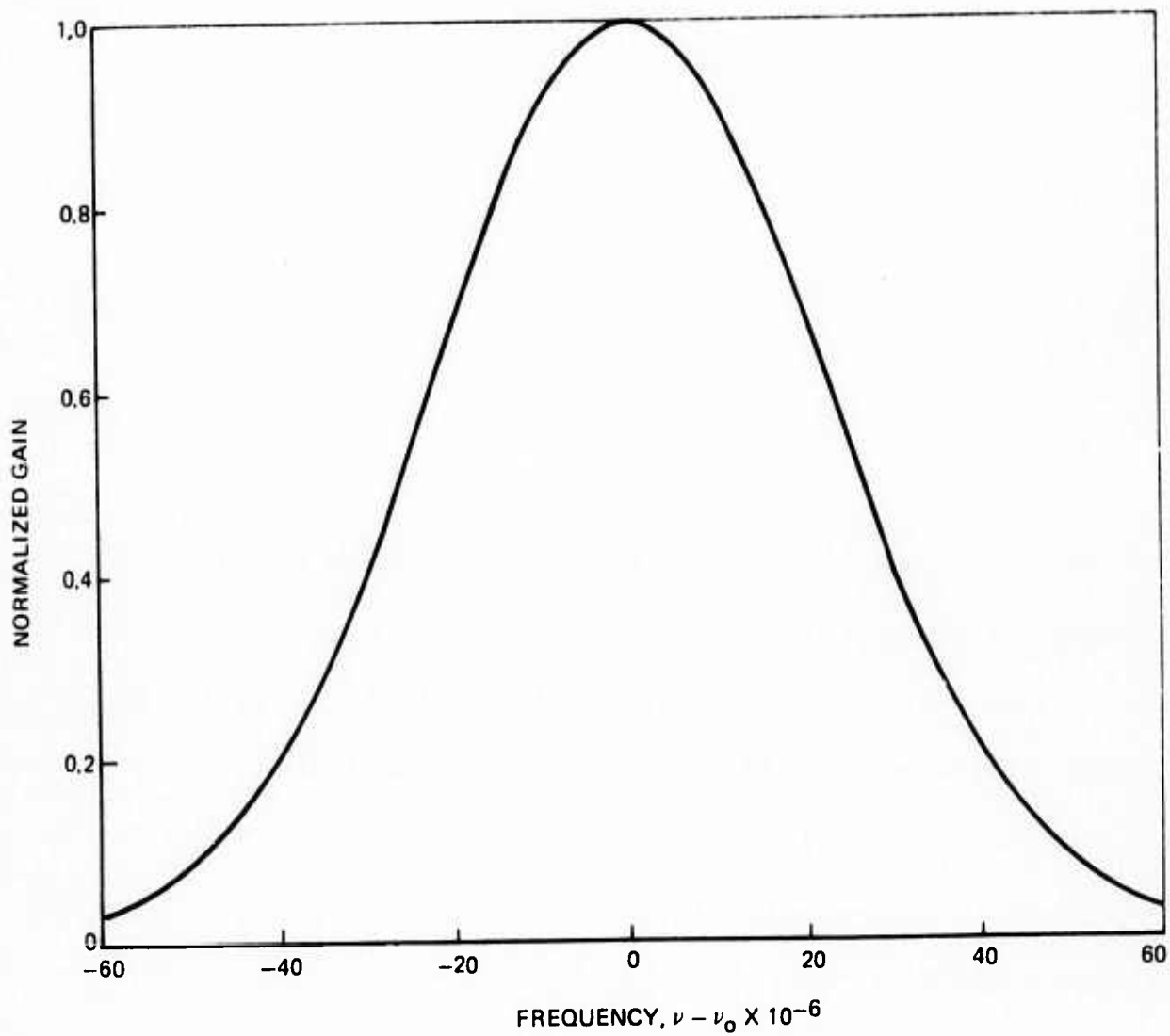


Figure 33. Normalized Gain in the Doppler Region as a Function of Frequency for  $T = 300^\circ\text{K}$

between the probe laser beam and bulk gas velocity vector will cause a 23 percent reduction in gain. The normalized gain is reduced from 1 to 0.77. A similar reduction in gain can also result if the probe laser operates at some frequency  $\nu$  instead of  $\nu_0$ . The magnitude of this second effect for the hypothetical example can also be estimated with figure 33 from the frequency difference  $(\nu - \nu_0)$ .

# REFERENCES

1. Bosov, N. G. and Oraevski, A. N., "Attainment of Negative Temperatures by Heating and Cooling of A System," Soviet Physics JETP, Vol. 17, No. 5, Nov. 1963, pp. 1171-1172.
2. Hurle, I. R. and Hertzberg, A., "Electronic Population Inversions by Fluid-Mechanical Techniques," The Physics of Fluids, Vol. 8, No. 9, Sept. 1965, pp. 1601-1607.
3. Konyukhov, V. K. and Prokhorov, A. M., "Population Inversion in Adiabatic Expansion of a Gas Mixture," JETP Letters, Vol. 3, No. 1, Jan. 1966, pp. 286-288.
4. Gerry, E. T., "Gas Dynamic CO<sub>2</sub> Lasers," American Physical Society Meeting Washington, D. C., April 1970.
5. Konyukhov, V. K., Mastrosov, I. V., Prokhorov, A. M., Shulunov, D. T., and Shirokov, N. N., "Gas-dynamic CW Laser Using a Mixture of Carbon Dioxide, Nitrogen, and Water," USSR Academy of Sciences, Zhurnal Eksperimental'noi i Tseroeticheskoi Fiziki, Pis'ma u Redaktsiyu, Vol. 12, Nov. 20, 1970, pp. 461-464.
6. Anderson, J. D., Jr., "Time-Dependent Analysis of Population Inversions in an Expanding Gas," The Physics of Fluids, Vol. 13, No. 8, Aug. 1970, pp. 1983-1989.
7. Anderson, J. D., Jr., "A Time-Dependent Quasi-One-Dimensional Analysis of Population Inversions in an Expanding Gas," NOLTR 69-200, Dec. 1969, Naval Ordnance Lab., White Oak, Silver Spring, Maryland.

8. Anderson, J. D., Jr., "Numerical Experiments Associated with Gas Dynamic Lasers," NOLTR 70-198, Sept. 1970, Naval Ordnance Lab., White Oak, Silver Spring, Maryland.
9. Meinzer, R. A., "Experimental Gas Dynamic Laser Studies," AIAA Journal 10, No. 4, April 1972, pp. 388-393.
10. Wilson, E. B., An Introduction to Scientific Research, McGraw-Hill Book Co., Inc., New York, 1952.
11. Scadron, M. D. and Warshawsky, I., "Experimental Determination of Time Constants and Nusselt Numbers for Bare-Wire Thermocouples in High-Velocity Air Streams and Analytic Approximation of Conduction and Radiation Errors," National Advisory Committee for Aeronautics, Technical Note 2599.
12. Weast, R. C. and Selby S. M., Handbook of Chemistry and Physics, The Chemical Rubber Co., Cleveland, Ohio, 1967.